AsCAN: Asymmetric Convolution-Attention Networks for Efficient Recognition and Generation

Anil Kag **Huseyin Coskun** **Jierun Chen**[*] **Junli Cao**
Willi Menapace **Aliaksandr Siarohin** **Sergey Tulyakov** **Jian Ren**
Snap Inc.
Project Page: https://snap-research.github.io/snap_image

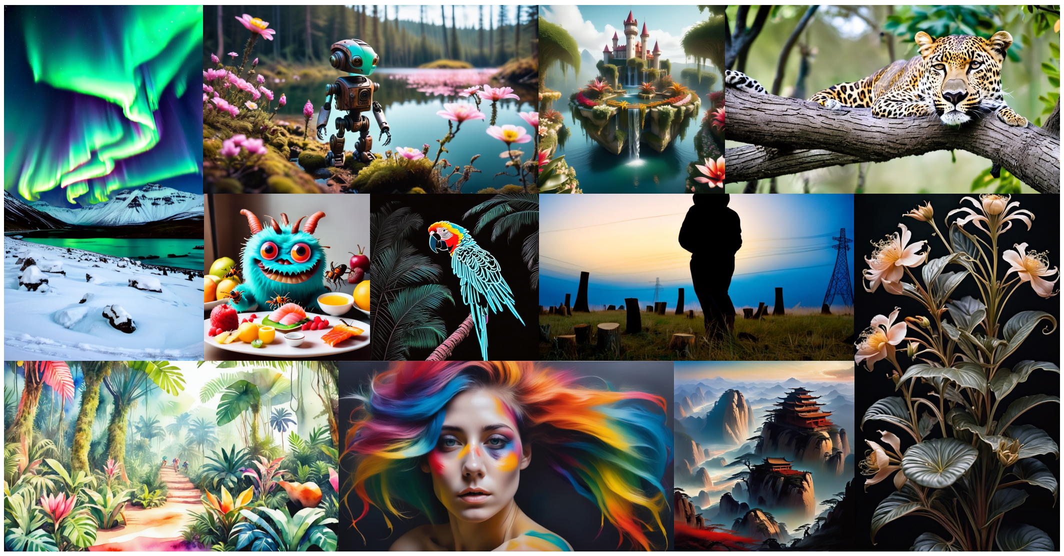
Figure 1: Example images generated by our efficient text-to-image generation model based on an asymmetric architecture. It generates photo-realistic images while following long prompts.

Abstract

Neural network architecture design requires making many crucial decisions. The common desiderata is that similar decisions, with little modifications, can be reused in a variety of tasks and applications. To satisfy that, architectures must provide promising latency and performance trade-offs, support a variety of tasks, scale efficiently with respect to the amounts of data and compute, leverage available data from other tasks, and efficiently support various hardware. To this end, we introduce AsCAN—a hybrid architecture, combining both convolutional and transformer blocks. We revisit the key design principles of hybrid architectures and propose a simple and effective *asymmetric* architecture, where the distribution of convolutional and transformer blocks is *asymmetric*, containing more convolutional blocks in the earlier stages, followed by more transformer blocks in later stages. AsCAN supports a variety of tasks: recognition, segmentation, class-conditional image generation, and features a superior trade-off between performance and latency. We then scale the same architecture to solve a large-scale text-to-image task and show state-of-the-art performance compared to the most recent public

[*]Work done during an internship at Snap Inc.

and commercial models. Notably, even without any computation optimization for transformer blocks, our models still yield faster inference speed than existing works featuring efficient attention mechanisms, highlighting the advantages and the value of our approach.

1 Introduction

Convolutional neural networks (CNNs) and transformers have been deployed in a wide spectrum of real-world applications, addressing various computer vision tasks, *e.g.*, image recognition [1, 2] and image generation [3, 4, 5, 6, 7, 8]. CNNs encode many desirable properties like translation equivariance facilitated through the convolutional operators [9]. However, they lack the input-adaptive weighting and the global receptive field capabilities offered by transformers [10, 11]. By recognizing the potential benefits of combining these complementary strengths, research endeavors explore *hybrid architectures* that integrate both convolutional and attention mechanisms [12, 13, 14, 15]. Recently, such architectures witness huge success when scaled up to train large-scale text-to-image (T2I) diffusion models [16, 17, 18, 19], enabling a vast range of visual applications, such as content editing [20, 21, 22, 23, 24, 25, 26] and video generation [27, 28, 29, 30].

One prominent research area for hybrid models involves the creation of building blocks that can effectively combine convolution and attention operators [31, 32]. While these efforts seek to use the strengths of both operators, their faster attention alternatives only approximate the global attention, leading to compromised model performance as lacking a global receptive field. Thus, they necessitate incorporating additional layers to compensate for the capacity reduction due to the attention approximation. On the other hand, minimal effort is directed toward optimizing the *entire* hybrid architecture. This raises the question: *Is the current macro design of hybrid architecture optimal?*

In this work, we propose a *simple* yet *effective* hybrid architecture, wherein the number of convolution and transformer blocks is *asymmetric* in different stages. Specifically, we adopt more convolutional blocks in the early stages, where the feature maps have relatively large spatial sizes, and more transformer blocks at the later stages. This design is verified across different tasks. For example, in Fig. 3, we demonstrate superior advantages of our model for the latency-performance trade-off on ImageNet-1K [33] classification task. Particularly, our model achieves even *faster speed* than many works featuring efficient attention operations. Additionally, we scale up our architecture to train the large-scale T2I diffusion model for high-fidelity generation (Fig. 1, Fig. 4, and Tab. 3). Furthermore, considering the high training cost for the large-scale T2I diffusion models, we introduce a multi-stage training pipeline to improve the training efficiency. Overall, our contributions can be summarized as follows:

- We revisit the macro design principles of hybrid convolutional-transformer architectures and propose one with asymmetrically distributed convolutional and transformer blocks.
- For the image classification task, we perform extensive latency analysis on the ImageNet-1K dataset and show our models achieve superior throughput-performance trade-offs than existing works (see Fig. 3). Notably, we show that the model runtime can be significantly accelerated *even without any acceleration optimization on attention operations*. Additionally, we show our pre-trained models on ImageNet-1K can be applied to downstream tasks such as semantic segmentation.
- For the class-conditional generation on ImageNet-1K (256×256), our asymmetric UNet achieves similar performance as state-of-the-art models with half the compute resources (see Tab. 4).
- For the text-to-image generation task, we demonstrate that our network can be scaled up for the large-scale T2I generation with a better performance-latency trade-off than existing public models (as in Tab. 3). Additionally, we improve the training efficiency through a multi-stage training pipeline, where we first train the model on a small dataset, *i.e.*, ImageNet-1K, for T2I generation, then fine-tune the model on a large-scale dataset.

2 Related Works

Efficient Hybrid Architectures. Over the past decade, convolutional neural networks (CNNs) [34, 35, 36] have achieved unprecedented performance in various computer vision tasks [37, 38]. Despite numerous attempts to improve CNNs [39, 40, 41, 42, 43], they still face limitations, particularly in terms of their local and restrictive receptive fields. On the other hand, the vision transformer (ViT) treats images as sequences of tokens [44], facilitating the computation of global dependencies between tokens to enhance the receptive field. However, ViTs come with quadratic computation complexity concerning input resolution. To address this, several studies have aimed to develop more efficient attention operations [45, 46, 47, 48, 49]. Recently, there has been a growing interest in exploring models that go beyond pure convolutional or transformer blocks, combining them within a single architecture to harness the spatial and translational priors from convolutions and the global receptive fields from the attention mechanism [11, 31, 2, 12, 32]. We revisit the design choices of hybrid architectures and propose a new design with a fast runtime while maintaining high performance. We reveal that optimizing the macro architecture directly allows us to use the original attention for a superior latency-performance trade-off compared to existing works. Most importantly, our designed networks can be applied to different domains, *e.g.*, image recognition and image generation, with both superior latency-performance trade-offs.

Text-to-Image Diffusion Models. The development of text-to-image models, such as GAN-based models [50, 7], autoregressive models [51, 52], and diffusion models [3, 53], has enabled the generation of high-fidelity images by using textual descriptions. Among them, diffusion models demonstrate advantages in stable training processes and the scalability of large-scale neural networks [19, 54, 55, 16, 17, 13]. Recent studies explore the enhancements of text-to-image diffusion models through various directions, such as designing new network architectures [56, 57, 58, 59, 60, 61, 62, 63], improving inference efficiency during multi-steps sampling [64, 65, 66], and accelerating the training convergence [67, 68, 69, 70, 71]. Our designed network can be scaled up for the T2I generation when modified to a UNet architecture [13]. The model achieves better performance-latency trade-offs than open-sourced models. Furthermore, we can reduce the training cost through the proposed two-stage training pipeline.

3 Methods

This section describes our network and training designs in detail. First, we justify our choices of utilizing the convolutional and transformer operations for the building blocks, which we then use to design the asymmetric architecture (Sec. 3.1). Second, we scale up the network architecture for training the text-to-image diffusion models (Sec. 3.3). We point out that it is easier to ablate the design of building blocks on the image classification task due to the lower resource requirements (training/evaluation compute) in comparison to image generation.

3.1 Architecture Design: Asymmetric Convolution-Attention Networks (AsCAN)

Our hybrid architecture consists of a mix of convolutional and transformer blocks, which enables operating on different input resolutions seamlessly and allows us to be pareto efficient *w.r.t.* performance-compute trade-off compared to other architectures. Before delving into the exact architecture configuration, we discuss our choice of the building blocks. We use $X \in \mathbb{R}^{H \times W \times C}$ to represent the input feature map X that has $H \times W$ spatial dimensions along with C channels. We denote $Y \in \mathbb{R}^{H' \times W' \times C'}$ as the output of a building block (convolution or transformer) and $\circ$ symbol for the function composition operator. In the following, we present our design choices based on ImageNet-1K [72] classification task by varying different convolution and transformer blocks.

Convolutional Block (`C`)**.** There are various choices for a convolutional block that can be used in our architecture, *e.g.*, MBConv [73], FusedMBConv [1], and ConvNeXt [74]. While MBConv block has been used in many networks [75, 31], the presence of depthwise convolutions results in low accelerator utilization for high-end GPUs [1]. To better understand the latency-performance trade-off for various convolutional blocks, we experiment with the *same* hybrid architecture yet with *different* convolutional blocks. As in Tab. 1 (more experimental settings in Sec. 4.1), FusedMBConv has better latency on A100 and V100 GPUs than others, while maintaining high performance. Therefore, we adopt FusedMBConv (`C`) for the convolutional block and represent it as $Y = X + \mathcal{P} \circ \mathcal{SE} \circ \mathcal{C}(X)$, where $\mathcal{C}$ is a full 3×3 convolution with $4\times$ channel expansion followed by batch norm and GeLU non-linearity [76], $\mathcal{SE}$ is a squeeze-and-excite operator [39] with shrink ratio of 0.25, and $\mathcal{P}$ is a 1×1 convolution to project to C channels.

Transformer Block (`T`)**.** Similar to the convolution blocks, there are many choices for attention mechanism in transformers, *e.g.*, blocks containing efficient attention mechanisms like multi-axial attention [31] and hierarchical attention [32]. Tab. 2 shows that vanilla attention mechanism provides

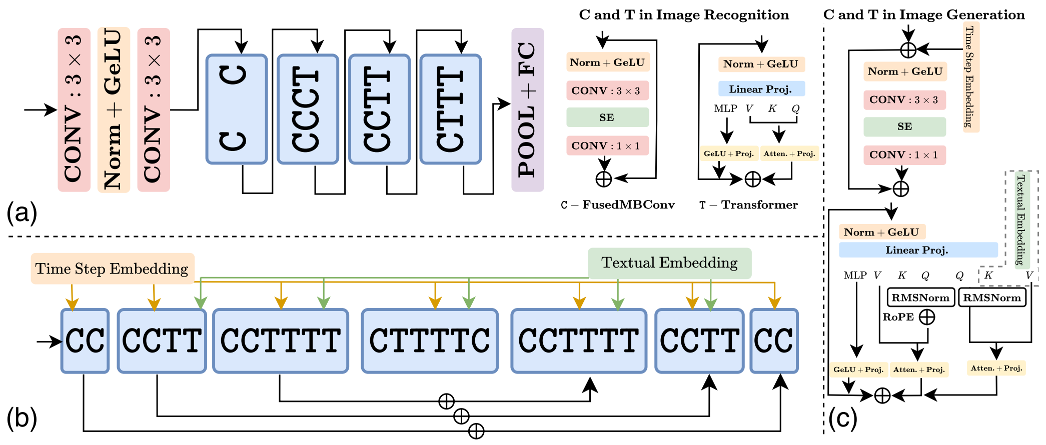

Figure 2: **Example AsCAN architectures for Image Classification & Text-to-Image Generation.** **(a):** The architecture for the image classification and details of the convolutional (C) and transformer blocks (T). AsCAN includes Stem (consisting of convolutional layers) and four stages followed by pooling and classifier. **(b):** The UNet architecture for the image generation. The Down blocks (the first three blocks starting from *left*) have the reverted reflection as the Up blocks (the first three blocks starting from *right*). **(c):** The details for C and T used in UNet. For the T that performs the cross attention between latent image features and textural embedding, the Q matrix comes from the textural embedding. Note that, compared to image classification, the C and T blocks for image generation only adds extra components to incorporate the input time-step and textual embeddings.

a better accuracy *vs* throughput trade-off across different GPUs and batch sizes. Thus, we choose the vanilla attention in our transformer block (T). We express it with the following update equations:

$$Y = X + Y_{\text{attn}} + Y_{\text{mlp}}; \;\; Y_{\text{attn}} = \mathcal{P} \circ \mathcal{A} \circ \mathcal{P}_{\text{QKV}}(\hat{X}); \;\; Y_{\text{mlp}} = \mathcal{P} \circ \phi \circ \mathcal{P}_{\text{MLP}}(\hat{X}), \tag{1}$$

where $\hat{X} = \mathcal{LN} \circ \phi(X)$, $\mathcal{LN}$ denotes layer normalization, ϕ denotes the GeLU non-linearity [76], $\mathcal{A}$ is the multi-headed self-attention function, $\mathcal{P}_{\text{QKV}}$ & $\mathcal{P}_{\text{MLP}}$ denote the linear projection to the QKV and MLP space, respectively, and $\mathcal{P}$ denotes the projection operator to the same space as the input. Note that these update equations are inspired by recent works [77, 78], where the feed-forward and the self-attention operators are arranged in parallel in order to get improved throughput with marginal reduction in performance.

Design Choices. Given the FusedMBConv (C) and Vanilla Transformer (T) blocks, we introduce the macro design for our hybrid architecture. For the image classification task, we follow the existing works [11, 31, 32] to utilize a four-stage architecture (excluding the convolutional Stem at the beginning and classifier components at the end). However, before finalizing our architecture, we still have a design question to answer, namely, *in which configuration should we arrange these building blocks?* For instance, CoAtNet [11] chooses to stack convolutional blocks in the first two stages and transformer blocks in the remaining stages while MaxViT [31] stacks convolutional and transformer blocks alternatively throughout the entire network. A formal algorithm requires evaluating all possible C and T configurations, which is computationally expensive. Even neural architecture search leads to exponential search space. Thus, we follow a naive strategy that is based on the following principles:

- C **before** T. In any stage, we prefer convolutions followed by transformer blocks to capture the global dependence between the features aggregated by the convolutions, as they can capture scale and translation-aware information. Our ablations in Appendix Tab. 9 justify this design choice.
- **Fixed first stage.** As transformer blocks have quadratic computation complexity in terms of the sequence length, we prefer the first stage to contain only convolutional blocks to improve the inference latency.
- **Equal blocks in remaining stages.** For ease of analysis, we fix the number of blocks in the remaining stages, *i.e.*, stages 2 to 4, to be four. Once we finalize the basic configuration, we can scale these stages similar to earlier works [31] to achieve larger models.
- **Asymmetric** *vs* **Symmetric.** We refer to the architectures as symmetric whenever C and T blocks are distributed equally within a stage. For example, a configuration of CCCC-CCTT-TTTT is

symmetric since both C and T blocks are equal within a stage. In contrast, the configuration of CCCT-CCTT-CTTT is asymmetric since C and T blocks are not equal in stages 2 and 4.

Final Architecture. Given these design principles, we list various promising configurations for the building blocks (C & T), and analyze their inference throughput and top-1 accuracy. Tab. 2 provides these configurations along with performance and runtime on different GPUs. For a better comparison with existing works, we also add the configurations of CoAtNet and MaxViT for reference. From the results, we can draw the following conclusions:

- Compared to symmetric architecture design, asymmetric distribution of C & T blocks yield a better trade-off for throughput and accuracy, as compared by configurations C1-C5 *vs* C6-C10.
- Higher number of transformer blocks in the early stages result in lower throughput, which can be observed by comparing the latency for the configurations of C2 *vs* C10, and C8 *vs* C9.
- While increasing the number of transformer blocks in the network improves the throughput, it does not result in improved accuracy, as demonstrated by C6 *vs* C9.

Given above analysis, we prefer the C1 configuration for simplicity along with better accuracy *vs* latency trade-off. Since transformer blocks capture global dependencies, we prefer at least some blocks in the early layers as well in conjunction with the convolutional blocks. Similarly, we prefer having few convolutional blocks in the later stages to capture the spatial, translation, or scale aware features. To be concrete, our final architecture includes a convolutional stem followed by four stages and the classifier head. In the first stage, we only keep convolutional blocks. In the second stage, we keep 75% convolutional and 25% transformer blocks. This trend is reversed in the final stage. For the third stage, we keep equal number of convolutional and transformer blocks. We visualize this configuration in Fig. 2 along with the diagrams representing the convolutional and transformer blocks.

Remarks. For simplicity, in this work, we focus on the configuration in which to combine the C & T blocks, and leverage vanilla quadratic attention and convolutional mechanisms. We can incorporate faster alternatives to quadratic attention to further boost the performance and latency trade-offs. We leave this exploration to future research.

3.2 Discussion

While many works in the literature focus on improving the trade-off between performance and multiply-add operation counts (MACs), most of the time, MACs do not translate to throughput gains. It is primarily due to the following reasons:

- *Excessive use of operations that do not contribute to MACs.* Such tensor operators include reshape, permute, concatenate, stack, etc. While these operations do not increase MACs, they burden the accelerator with tensor rearrangement. The cost of such rearrangement grows with the size of the feature maps. Thus, whenever these operations occur frequently, the throughput gains drop significantly. For instance, MaxViT [31] uses axial attention that includes many permute operations for window/grid partitioning of the spatial features. Similarly, SMT [79] includes many concatenation and reshape operations in the SMT-Block. It reduces the throughput significantly even though their MACs are lower than AsCAN (see Appendix Tab. 7).
- *MACs do not account for non-linear accelerator behavior in batched inference.* Another issue is that MACs do not account for the non-linear behavior of the GPU accelerators in the presence of larger batch sizes. For instance, with small batch sizes (B=1), the GPU accelerator is not fully utilized. Thus, the benchmark at this batch size is not enough. Instead, one should benchmark at larger batch sizes to see consistency between architectures.
- *Lack of efficient CUDA operators for specialized building blocks.* Many architectures propose specialized and complex attention or convolution building blocks. While these blocks offer better MACs-vs-performance trade-offs, it is likely that their implementation relies on naive CUDA constructs and does not result in significant throughput gains. For instance, Bi-Former [80] computes attention between top-k close regions using a top-k sorting operation and performs many gather operations on the queries and keys. Similarly, RMT [81] computes the Manhattan distance between the tokens in the image. It includes two separate attention along the height and width of the image. This process invokes many small kernels along with reshape and permute operations. These specialized blocks would benefit from efficient CUDA kernels.
- *Using accelerator-friendly operators.* Depending on the hardware, some operators are better than others. Depth-wise separable convolutions reduce the MACs, yet they may not be efficient for

Table 1: **Analysis of the Configuration of Convolution and Transformer Blocks.** We analyze various convolutional and transformer blocks by training hybrid architectures with different options on the ImageNet-1K dataset. We provide the inference latency (as throughput) for different GPUs. Results show that FusedMBConv and Vanilla Transformer blocks provide a better trade-off over accuracy and latency than others.

Convolution-Based Block	Params	(Images/s) A100 B=64	(Images/s) V100 B=16	Top-1 Acc.
MBConv	29M	3013	914	83.12%
ConvNext	35M	3923	1104	82.81%
FusedMBConv	55M	4295	1148	83.44%

Transformer-Based Block	Params	(Images/s) A100 B=64	(Images/s) V100 B=16	Top-1 Acc.
Multi-Axial	83M	3541	630	83.59%
Hierarchical	74M	3470	552	83.51%
Vanilla	55M	4295	1148	83.44%

Table 2: **Analysis of Architecture Configuration.** We analyze the distribution of convolution and transformer blocks by training hybrid architecture with different distributions of blocks on ImageNet-1K dataset [72]. It demonstrates that the design in Fig. 2 provides a better trade-off over accuracy and latency. Symbol `M` denotes MaxViT block [31] composed of MBConv[73, 75] and Multi-Axial Attention blocks, which is equivalent to `CT`. Note that CoAtNet [11] uses MBConv blocks compared to the FusedMBConv blocks in our design.

Family	Block Configuration	Params	Inference(images/s) A100 B=16	Inference(images/s) A100 B=64	Inference(images/s) V100 B=16	Top-1 Acc.
Our	`CC-CCCT-CCTT-CTTT` (C1)	55M	3224	4295	1148	83.4%
	`CC-CCCT-CCTT-CCTT` (C2)	73M	3217	4179	1036	83.2%
Asymmetric	`CC-CCCT-CCTT-TTTT` (C3)	41M	3384	4472	1224	82.9%
	`CC-CCCT-CCCC-TTTT` (C4)	50M	3434	4411	1182	83.1%
	`CC-CCCT-CCCT-CCCT` (C5)	95M	3135	4066	991	82.7%
Our	`CC-CCCC-CCCC-TTTT` (C6)	51M	3783	4998	1280	82.8%
	`CC-CCCC-CCTT-TTTT` (C7)	42M	3536	4941	1296	82.4%
Symmetric	`CC-CCCC-TTTT-TTTT` (C8)	34M	3475	5311	1469	82.6%
	`CC-TTTT-TTTT-TTTT` (C9)	30M	3216	4091	1293	82.7%
	`CC-CCTT-CCTT-CCTT` (C10)	72M	2942	3820	980	82.8%
CoAtNet-0	`CC-CCC-TTTTT-TT`	25M	3537	5221	976	81.6%
CoAtNet-1	`CC-CCCCCC-TTTTTTTTTTTTTT-TT`	42M	2221	2907	629	83.3%
MaxViT-T	`MM-MM-MMMMM-MM`	31M	1098	2756	357	83.6%

particular hardware. Excessive use of depth-wise separable convolutions should be avoided in favor of the full convolutions wherever possible. For instance, MogaNet [82] extensively uses depth-wise convolutions with large kernel sizes and concatenation operations. These operators reduce the multiply-addition counts, which are not necessarily efficient on high-end GPU accelerators.

3.3 Scaling Up Architecture for Image Generation

We further scale up our architecture for the image generation task, which requires more computation than the image recognition task. We train our network by utilizing the denoising diffusion probabilistic models (DDPM) [16, 17, 54] in the latent space [13]. The latent diffusion model includes a variational autoencoder (VAE) [83, 84] that encodes the image $\mathbf{x}$ into latent $\mathbf{z}$ and a diffusion model $\hat{\boldsymbol{\epsilon}}_{\boldsymbol{\theta}}(\cdot)$ with parameters $\boldsymbol{\theta}$. We utilize UNet [18] as the network for the diffusion model. For the T2I generation, we get the text embedding with Flan-T5-XXL encoder [85]. We train the diffusion model following the noise prediction [16, 17]:

$$\min_{\boldsymbol{\theta}} \mathbb{E}_{t\sim[1,T],\boldsymbol{\epsilon}\sim\mathcal{N}(\mathbf{0},\mathbf{I})} \left\|\boldsymbol{\epsilon} - \hat{\boldsymbol{\epsilon}}_{\boldsymbol{\theta}}(\mathbf{z}_t, \mathbf{c})\right\|^2, \tag{2}$$

where t is the time step and T is the total number of steps, $\boldsymbol{\epsilon}$ is the added Gaussian noise, and $\mathbf{c}$ is the condition signal. $\mathbf{z}_t$ is a noisy latent obtained with a pre-defined variance schedule $\{\beta_t \in (0,1)\}_t$ with the following updates [16]:

$$\mathbf{z}_t = \sqrt{\bar{\alpha}_t}\mathbf{z} + \sqrt{1-\bar{\alpha}_t}\boldsymbol{\epsilon}; \quad \alpha_t = 1 - \beta_t; \quad \bar{\alpha}_t = \prod_{i=1}^{t} \alpha_i. \tag{3}$$

In the following, we discuss our design for the diffusion model and the multi-stage training pipeline.

3.3.1 Asymmetric UNet Architecture

We follow the existing literature [13, 8, 15, 86] to design the UNet architecture for the T2I diffusion model. Fig. 2 gives an overview of the overall architecture. It consists of three main stages, namely, Down blocks, Middle Block, and Up blocks. The Up blocks are the reverted reflection of the Down blocks. In addition, there are skip connections to add the features from Down blocks to Up blocks. We adopt the VAE from SDXL [8] to transform the image to the latent space and carry out the diffusion in this space. Since the text-to-image generation task requires additional inputs (*i.e.*, time and text embeddings), we modify the `C` and `T` blocks to incorporate these conditions. Similar to the existing literature [8], we add the time embedding to the `C` blocks. Additionally, we add the text embedding to the `T` blocks through a cross-attention operation carried in parallel to the self-attention operation as shown in Fig. 2(c).

While the UNet can take arbitrary resolution as input, we notice that adding positional embeddings in the self-attention operation reduces the artifacts such as duplicate patterns. For this purpose, we add RoPE [87] embeddings for encoding the position information in the `T` blocks. Further, we incorporate query-key normalization using the RMSNorm [88] for stable training in lower precision (`bfloat16`).

3.3.2 Improved Multi-Stage Training Pipeline

Instead of training the T2I network from scratch, we first train the model on a small-scale dataset and then fine-tune the model on a much larger dataset. It effectively reduces the training cost on the large-scale scale dataset (see ablation in Appendix Sec. A.6 , Fig 8). This strategy differs from existing works that perform multi-stage training using different architectures. For instance, PixArt-α [69, 71] trains a class conditional image generation network and modifies it to fine-tune the network for text-to-image generation. Both our pre-training and fine-tuning tasks use the same architecture for text-to-image generation. We use the AdamW optimizer [89] with $\beta_1 = 0.9$ and $\beta_2 = 0.99$.

Specifically, in the first stage, we train our model using ImageNet-1K [33] for the text-to-image generation. Following Esser *et al.* [90], we form the conditioned text prompt as "a photo of a `<class name>`", where `class name` is randomly chosen from the label of each image. The model is trained to generate an image with a resolution of 256×256. In the second stage, we fine-tune the model from the first stage on a much larger dataset. Here we train the model in four phases: First, we conduct training at the resolution of 256×256 for 300K iterations with the batch size as $16,384$ and $4e-4$ as the learning rate. Second, we continue the training at the resolution of 512×512 for 200K iterations with the batch size as $6,144$ and $1e-4$ as the learning rate. Third, we train the model for 1024×1024 for 100K iterations with the batch size as $1,536$ and $5e-5$ as the learning rate. Finally, we perform the multi-aspect ratio training such that the model can synthesize images at various resolution [8]. Additionally, we adjust the added noise at different resolution [15], *i.e.*, β_T in Eq. (3) is chosen as 0.01 for 256×256 and 0.02 for higher resolution (see ablations in Appendix Sec. A.6). We add an offset noise of 0.05 during multi-aspect ratio training similar to earlier works[8].

4 Experiments

In this section, we evaluate the architectures proposed in Sec. 3.1 on image recognition and generation tasks. We also apply this design to the semantic segmentation task in Appendix Sec. A.3. We highlight the important aspects of these experiments below and provide the experimental details in the appendix.

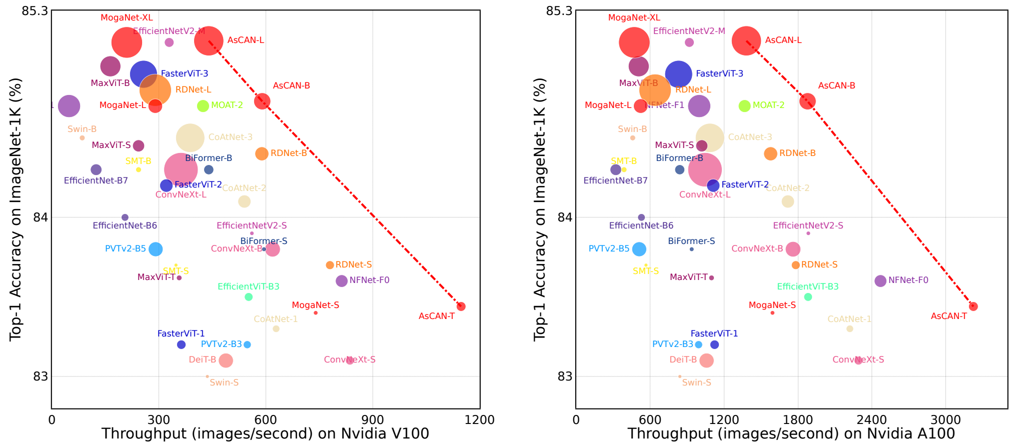

Figure 3: **Top-1 Accuracy *vs* Inference Latency on ImageNet-1K Classification.** We plot the latency measured as images inferred per second on a single V100 GPU (*Left*)/A100 GPU (*Right*) with batch-size 16 with 224×224 resolution. The plot compares state-of-the-art models (convolutional, transformer, hybrid architectures) against the proposed AsCAN architecture. The area of each circle is proportional to the model size. Our model consistently achieves better accuracy *vs* latency trade-offs. While some models regress between two hardware (*e.g.*, MaxViT-S vs SMT-B), our model consistently achieves better accuracy *vs* latency trade-offs. We report additional baselines along with multiply-add operations count and different batch sizes in Appendix Tab. 7.

4.1 Image Recognition

We scale the AsCAN architecture discussed in Sec. 3.1 to base and large variants following earlier works [31]. We train these variants on the ImageNet-1K[72] classification task. We provide the experimental details (dataset description, architectures, training hyper-parameters) in Appendix Sec. A.2. Fig. 3 plots the inference speed on a V100 GPU with batch size 16 (measured in images processed per second) and top-1 accuracy achieved on this task for various models. In addition, Appendix Tab. 7 shows the parameter count and inference speed on both V100 and A100 GPUs along with additional details such as floating-point multiply-add count (FLOPs/MACs) and inference speed across different batch sizes. Below, we highlight the salient observations from these experiments.

- *More than* $2\times$ *higher throughput across accelerators.* Compared to the existing hybrid architectures such as FasterViT [32] and MaxViT [31], the proposed AsCAN family achieves similar or better top-1 accuracy with more than $2\times$ higher throughput. This trend holds true for both A100 and V100 GPUs. For instance, on A100 with batch=16, FasterViT-1 achieves 83.2% top-1 accuracy with throughput as 1123 images/s, while AsCAN-T has 83.44% with throughput as 3224 images/s.
- *Better throughput across different batch sizes.* AsCAN consistently achieves better throughput across batch sizes for both the accelerators compared to baselines.
- *Better storage and computational footprint.* AsCAN-family of architectures requires less number of parameters and float operations to achieve similar performance. For example, to achieve nearly 85.2% accuracy, MaxViT-L requires 212M parameters and 43.9G MACs whereas AsCAN-L requires 173M parameters and 30.7G MACs.
- We achieve better latency *vs.* accuracy trade-off than hybrid architectures with better alternatives to the attention mechanisms in transformer. For instance, we outperform newer architectures such as PVTv2[91], MOAT[92], EfficientViT[93], and Scale-Aware Modulation Transformers[79].

Further, we observe similar trends when we scale these models to pre-training on *ImageNet-21K* [94] dataset (see Appendix Sec. A.2.3) as well as semantic *segmentation* task (Appendix A.3).

Table 3: **GenEval Scores.** We use this benchmark to compare T2I models on various aspects of generation, including counting, color attribution, position, etc. It clearly shows that our model achieves better overall score, by convincingly outperforming pipelines such as PixArt-α and SDXL.

Model	Overall	Single Object	Two Objects	Counting	Colors	Position	Color Attribution
SDv1.5	0.43	0.97	0.38	0.38	0.76	0.04	0.06
PixArt-α	0.48	0.98	0.50	0.44	0.80	0.08	0.07
SDv2.1	0.50	0.98	0.51	0.44	0.85	0.07	0.17
PixArt-Σ	0.53	0.99	0.65	0.46	0.82	0.12	0.12
SDXL	0.55	0.98	0.74	0.39	0.85	0.15	0.23
Ours	0.64	0.99	0.78	0.43	0.88	0.28	0.48

4.2 Class Conditional Generation

We apply our asymmetric UNet architecture to learn class conditional image generation on the ImageNet-1K dataset with 256×256 resolution. We train a smaller variant of our asymmetric UNet architecture (as in Sec. 3.3.1) with nearly 400M parameters and inject the class condition through cross-attention mechanism. We train this model using DDPM [16] (more details in Appendix Sec. A.7), and provide results in Tab. 4. As can be seen, we achieve Fréchet Inception Distance (FID) [95] close to state-of-the-art models with nearly half the FLOPs (*e.g.*, Ours *vs.* DiT-XL/2-G), and better FID than the existing work with similar computation (*e.g.*, Ours *vs.* U-ViT-L/2).

4.3 Text-to-Image Generation

Below, we evaluate our T2I asymmetric UNet architecture trained using the multi-stage training.

GenEval Benchmark. We evaluate our model on the GenEval [97] benchmark that studies various aspects of an image generation model. Tab. 3 shows that our model outperforms fast training pipelines such as PixArt-α by a significant margin. It beats even larger models such as SDXL which consume significantly more training data and computational resources.

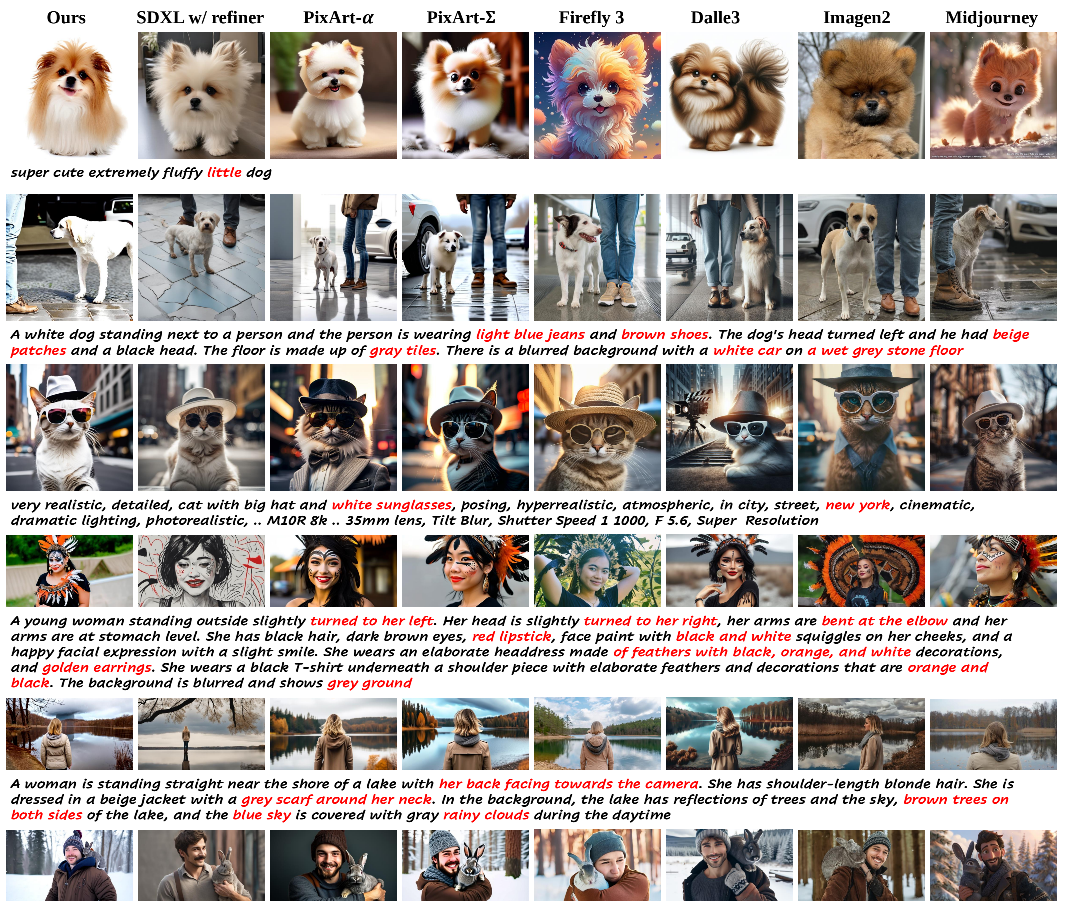

super cute extremely fluffy little dog

A white dog standing next to a person and the person is wearing light blue jeans and brown shoes. The dog's head turned left and he had beige patches and a black head. The floor is made up of gray tiles. There is a blurred background with a white car on a wet grey stone floor

very realistic, detailed, cat with big hat and white sunglasses, posing, hyperrealistic, atmospheric, in city, street, new york, cinematic, dramatic lighting, photorealistic, .. M10R 8k .. 35mm lens, Tilt Blur, Shutter Speed 1 1000, F 5.6, Super Resolution

A young woman standing outside slightly turned to her left. Her head is slightly turned to her right, her arms are bent at the elbow and her arms are at stomach level. She has black hair, dark brown eyes, red lipstick, face paint with black and white squiggles on her cheeks, and a happy facial expression with a slight smile. She wears an elaborate headdress made of feathers with black, orange, and white decorations, and golden earrings. She wears a black T-shirt underneath a shoulder piece with elaborate feathers and decorations that are orange and black. The background is blurred and shows grey ground

A woman is standing straight near the shore of a lake with her back facing towards the camera. She has shoulder-length blonde hair. She is dressed in a beige jacket with a grey scarf around her neck. In the background, the lake has reflections of trees and the sky, brown trees on both sides of the lake, and the blue sky is covered with gray rainy clouds during the daytime

In the daytime, a young man standing slightly turned to his right, while holding a gray rabbit behind his left shoulder. His right arm is bent at the elbow and resting on his left shoulder, while his left arm is down and his head turned to the right. He has a stubbled mustache, a beard, grey eyes and a happy facial expression with a wide smile. He is wearing a gray knitted hat with dark blue-brown patterns, a dark brown jacket, and a black sweater. There is a snowy forest with snow-capped trees in the background.

Figure 4: **Qualitative Comparison against open source and commercial models.** We compare our T2I model against generations from different baselines. We illustrate that many times existing models generate images with less photo-realism (either lot less details or more on the cartoonish side), specially for PixArt-α and PixArt-Σ. Further, they frequently miss the fine-grained details explicitly asked in the prompts. We highlight these mistakes in red color in the input prompt. For instance, in the above generations (ordered A $\rightarrow$ F from top to bottom row), baselines miss details such as, (A) lack of realism (B) light blue jeans, (C) white sunglasses, (D) black, orange, and white feathers, (E) grey scarf & back towards camera, and (F) gray knitted hat with dark blue-brown patterns.

Qualitative Comparison. Fig. 4 shows a qualitative comparison between different methods. We highlight salient differences between the baselines and our generations. Baselines such as PixArt-α and PixArt-Σ tend to generate images with much less photo-realism and more often it is much more on the cartoonish side or it has grainy artifacts. Similarly, SDXL with refiner framework is unable to adapt to long text prompts due to limitations of the CLIP text-encoder. Hence, it misses many key features described in the prompts. In contrast, our model is able to follow the long prompts while adhering to the required semantics as well as photo-realism.

Human Preference study. We perform a user study to compare open-sourced models to evaluate their image-text alignment characteristics. We select 1000 prompts from our validation set and generate images from SDXL, PixArt-α, PixArt-Σ, and our multi-aspect ratio model. We show these results in the Fig. 5. It shows that our model convincingly outperforms both SDXL and PixArt-α generations, while it has similar image-text alignment as PixArt-Σ model. To further evaluate these models, we generate 10K images from our validation set (described in Appendix A.5.2) and compute the FID [95] between the generated and original images. We show these scores in Tab. 5, which

Table 4: **ImageNet-1K Class Conditional Generation.** We train a smaller variant of our T2I UNet architecture to perform class conditional generation on ImageNet-1K. We train this model at 256×256 and 512×512. Our asymmetric architecture achieves similar FID as the state-of-the-art models with less than half the floating point operations (*e.g.*, Ours *vs.* DiT-XL/2-G), and better FID than the existing work with similar computation (*e.g.*, Ours *vs.* U-ViT-L/2).

	256×256			512×512		
Model	FLOPs	Throughput A100 (B=64) samples/sec	FID	FLOPs	Throughput A100 (B=64) samples/sec	FID
ADM [18]	110G	-	10.60	-	-	-
LDM [13]	104G	362	3.60	-	-	-
U-ViT-L/2 [86]	77G	498	3.40	340G	86	4.67
U-ViT-H/2 [86]	133G	271	2.29	546G	45	4.05
DiT-XL/2-G [4]	118G	293	2.27	525G	51	3.04
Ours	52G	556	2.41	224G	130	3.28
Ours (sampled cfg [96])	52G	556	2.23	224G	130	3.15

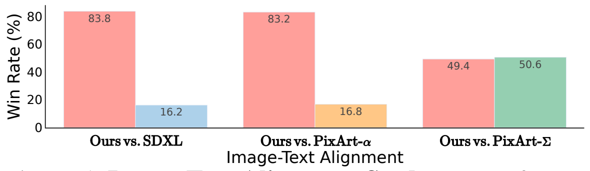

Figure 5: **Image-Text Alignment Study.** We perform user study for 1000 prompts and ask them to choose images with better image-text alignment. It shows that we outperform SDXL and PixArt-α. While our performance is on par with PixArt-Σ, Tab. 5 shows that we yield more realistic generations.

Table 5: **Validation Data Evaluation.** We use the validation set of captioned data for computing the FID scores for comparison between different models (see details in Appendix A.5.2)

Model	FID Set-B-10K	FID Set-A-10K
PixArt-α	46.03	20.12
PixArt-Σ	40.01	19.25
SDXL	35.86	16.49
Ours	15.45	10.88

clearly indicates that our generations align well with the real-world images. This is also evident from our earlier comparison on qualitative visualization in Fig. 4.

Resource Efficiency. We compare the resource requirements of our model against various baselines in Appendix Tab. 12. It shows that we achieve better inference latency compared to many existing models. Further, we consume considerably less compute to achieve much better performance than many existing baselines as illustrated by evaluations in the previous section.

5 Conclusion

In this work, we design hybrid architectures comprising convolutional and transformer blocks with applications to many computer vision tasks. We focus on developing a simple hybrid model with better throughput and performance trade-offs. Instead of designing efficient alternatives to the convolutional and transformer (mainly attention mechanism) blocks, we leverage existing vanilla attention along with the FusedMBConv block to design the new architecture, called AsCAN. Our main philosophy revolves around the uneven distribution of the convolutional and transformer blocks in the different stages of the network. We refer to this distribution as *asymmetric*, in the sense that it favors more convolutional blocks in the early stages with a mix of few transformer blocks, while it reverses this trend favoring more transformer blocks in the later stages with fewer convolutional blocks. We demonstrate the superiority of the proposed architecture through extensive evaluations across the image recognition task, class conditional generation, and text-to-image generation.

References

[1] Mingxing Tan and Quoc Le. Efficientnetv2: Smaller models and faster training. In *International conference on machine learning*, pages 10096–10106. PMLR, 2021.

[2] Yanyu Li, Geng Yuan, Yang Wen, Ju Hu, Georgios Evangelidis, Sergey Tulyakov, Yanzhi Wang, and Jian Ren. Efficientformer: Vision transformers at mobilenet speed. *Advances in Neural Information Processing Systems*, 35:12934–12949, 2022.

[3] Chitwan Saharia, William Chan, Saurabh Saxena, Lala Li, Jay Whang, Emily L Denton, Kamyar Ghasemipour, Raphael Gontijo Lopes, Burcu Karagol Ayan, Tim Salimans, et al. Photorealistic text-to-image diffusion models with deep language understanding. *Advances in Neural Information Processing Systems*, 35:36479–36494, 2022.

[4] William Peebles and Saining Xie. Scalable diffusion models with transformers. In *Proceedings of the IEEE/CVF International Conference on Computer Vision*, pages 4195–4205, 2023.

[5] Yanyu Li, Huan Wang, Qing Jin, Ju Hu, Pavlo Chemerys, Yun Fu, Yanzhi Wang, Sergey Tulyakov, and Jian Ren. Snapfusion: Text-to-image diffusion model on mobile devices within two seconds. *arXiv preprint arXiv:2306.00980*, 2023.

[6] Xian Liu, Jian Ren, Aliaksandr Siarohin, Ivan Skorokhodov, Yanyu Li, Dahua Lin, Xihui Liu, Ziwei Liu, and Sergey Tulyakov. Hyperhuman: Hyper-realistic human generation with latent structural diffusion. *arXiv preprint arXiv:2310.08579*, 2023.

[7] Minguk Kang, Jun-Yan Zhu, Richard Zhang, Jaesik Park, Eli Shechtman, Sylvain Paris, and Taesung Park. Scaling up gans for text-to-image synthesis. In *Proceedings of the IEEE/CVF Conference on Computer Vision and Pattern Recognition*, pages 10124–10134, 2023.

[8] Dustin Podell, Zion English, Kyle Lacey, Andreas Blattmann, Tim Dockhorn, Jonas Müller, Joe Penna, and Robin Rombach. Sdxl: Improving latent diffusion models for high-resolution image synthesis. *arXiv preprint arXiv:2307.01952*, 2023.

[9] Risi Kondor and Shubhendu Trivedi. On the generalization of equivariance and convolution in neural networks to the action of compact groups. In *International Conference on Machine Learning*, pages 2747–2755. PMLR, 2018.

[10] Alexey Dosovitskiy, Lucas Beyer, Alexander Kolesnikov, Dirk Weissenborn, Xiaohua Zhai, Thomas Unterthiner, Mostafa Dehghani, Matthias Minderer, Georg Heigold, Sylvain Gelly, Jakob Uszkoreit, and Neil Houlsby. An image is worth 16x16 words: Transformers for image recognition at scale. In *International Conference on Learning Representations*, 2021.

[11] Zihang Dai, Hanxiao Liu, Quoc V Le, and Mingxing Tan. Coatnet: Marrying convolution and attention for all data sizes. In A. Beygelzimer, Y. Dauphin, P. Liang, and J. Wortman Vaughan, editors, *Advances in Neural Information Processing Systems*, 2021.

[12] Yanyu Li, Ju Hu, Yang Wen, Georgios Evangelidis, Kamyar Salahi, Yanzhi Wang, Sergey Tulyakov, and Jian Ren. Rethinking vision transformers for mobilenet size and speed. In *Proceedings of the IEEE/CVF International Conference on Computer Vision*, pages 16889–16900, 2023.

[13] Robin Rombach, Andreas Blattmann, Dominik Lorenz, Patrick Esser, and Björn Ommer. High-resolution image synthesis with latent diffusion models. In *Proceedings of the IEEE/CVF Conference on Computer Vision and Pattern Recognition*, pages 10684–10695, 2022.

[14] Hao Li, Yang Zou, Ying Wang, Orchid Majumder, Yusheng Xie, R Manmatha, Ashwin Swaminathan, Zhuowen Tu, Stefano Ermon, and Stefano Soatto. On the scalability of diffusion-based text-to-image generation. *arXiv preprint arXiv:2404.02883*, 2024.

[15] Emiel Hoogeboom, Jonathan Heek, and Tim Salimans. simple diffusion: End-to-end diffusion for high resolution images. In *International Conference on Machine Learning*, pages 13213–13232. PMLR, 2023.

[16] Jonathan Ho, Ajay Jain, and Pieter Abbeel. Denoising diffusion probabilistic models. *Advances in Neural Information Processing Systems*, 33:6840–6851, 2020.

[17] Yang Song, Jascha Sohl-Dickstein, Diederik P Kingma, Abhishek Kumar, Stefano Ermon, and Ben Poole. Score-based generative modeling through stochastic differential equations. *arXiv preprint arXiv:2011.13456*, 2020.

[18] Prafulla Dhariwal and Alexander Nichol. Diffusion models beat gans on image synthesis. *Advances in Neural Information Processing Systems*, 34:8780–8794, 2021.

[19] Tero Karras, Miika Aittala, Timo Aila, and Samuli Laine. Elucidating the design space of diffusion-based generative models. *Advances in Neural Information Processing Systems*, 35:26565–26577, 2022.

[20] Alex Nichol, Prafulla Dhariwal, Aditya Ramesh, Pranav Shyam, Pamela Mishkin, Bob McGrew, Ilya Sutskever, and Mark Chen. Glide: Towards photorealistic image generation and editing with text-guided diffusion models. *arXiv preprint arXiv:2112.10741*, 2021.

[21] Chitwan Saharia, William Chan, Huiwen Chang, Chris Lee, Jonathan Ho, Tim Salimans, David Fleet, and Mohammad Norouzi. Palette: Image-to-image diffusion models. In *ACM SIGGRAPH 2022 Conference Proceedings*, pages 1–10, 2022.

[22] Aditya Ramesh, Prafulla Dhariwal, Alex Nichol, Casey Chu, and Mark Chen. Hierarchical text-conditional image generation with clip latents. *arXiv preprint arXiv:2204.06125*, 2022.

[23] Huiwen Chang, Han Zhang, Jarred Barber, AJ Maschinot, Jose Lezama, Lu Jiang, Ming-Hsuan Yang, Kevin Murphy, William T Freeman, Michael Rubinstein, et al. Muse: Text-to-image generation via masked generative transformers. *arXiv preprint arXiv:2301.00704*, 2023.

[24] Yogesh Balaji, Seungjun Nah, Xun Huang, Arash Vahdat, Jiaming Song, Karsten Kreis, Miika Aittala, Timo Aila, Samuli Laine, Bryan Catanzaro, et al. ediffi: Text-to-image diffusion models with an ensemble of expert denoisers. *arXiv preprint arXiv:2211.01324*, 2022.

[25] Zhixing Zhang, Ligong Han, Arnab Ghosh, Dimitris N Metaxas, and Jian Ren. Sine: Single image editing with text-to-image diffusion models. In *Proceedings of the IEEE/CVF Conference on Computer Vision and Pattern Recognition*, pages 6027–6037, 2023.

[26] Shelly Sheynin, Adam Polyak, Uriel Singer, Yuval Kirstain, Amit Zohar, Oron Ashual, Devi Parikh, and Yaniv Taigman. Emu edit: Precise image editing via recognition and generation tasks. *arXiv preprint arXiv:2311.10089*, 2023.

[27] Jonathan Ho, William Chan, Chitwan Saharia, Jay Whang, Ruiqi Gao, Alexey Gritsenko, Diederik P Kingma, Ben Poole, Mohammad Norouzi, David J Fleet, et al. Imagen video: High definition video generation with diffusion models. *arXiv preprint arXiv:2210.02303*, 2022.

[28] Agrim Gupta, Lijun Yu, Kihyuk Sohn, Xiuye Gu, Meera Hahn, Li Fei-Fei, Irfan Essa, Lu Jiang, and José Lezama. Photorealistic video generation with diffusion models. *arXiv preprint arXiv:2312.06662*, 2023.

[29] Rohit Girdhar, Mannat Singh, Andrew Brown, Quentin Duval, Samaneh Azadi, Sai Saketh Rambhatla, Akbar Shah, Xi Yin, Devi Parikh, and Ishan Misra. Emu video: Factorizing text-to-video generation by explicit image conditioning. *arXiv preprint arXiv:2311.10709*, 2023.

[30] Willi Menapace, Aliaksandr Siarohin, Ivan Skorokhodov, Ekaterina Deyneka, Tsai-Shien Chen, Anil Kag, Yuwei Fang, Aleksei Stoliar, Elisa Ricci, Jian Ren, et al. Snap video: Scaled spatiotemporal transformers for text-to-video synthesis. *arXiv preprint arXiv:2402.14797*, 2024.

[31] Zhengzhong Tu, Hossein Talebi, Han Zhang, Feng Yang, Peyman Milanfar, Alan Bovik, and Yinxiao Li. Maxvit: Multi-axis vision transformer. *ECCV*, 2022.

[32] Ali Hatamizadeh, Greg Heinrich, Hongxu Yin, Andrew Tao, Jose M Alvarez, Jan Kautz, and Pavlo Molchanov. Fastervit: Fast vision transformers with hierarchical attention. *arXiv preprint arXiv:2306.06189*, 2023.

[33] Jia Deng, Wei Dong, Richard Socher, Li-Jia Li, Kai Li, and Li Fei-Fei. Imagenet: A large-scale hierarchical image database. In *2009 IEEE conference on computer vision and pattern recognition*, pages 248–255. Ieee, 2009.

[34] Kaiming He, Xiangyu Zhang, Shaoqing Ren, and Jian Sun. Deep residual learning for image recognition. In *Proceedings of the IEEE conference on computer vision and pattern recognition*, pages 770–778, 2016.

[35] Alex Krizhevsky, Ilya Sutskever, and Geoffrey E Hinton. Imagenet classification with deep convolutional neural networks. *Advances in neural information processing systems*, 25, 2012.

[36] Karen Simonyan and Andrew Zisserman. Very deep convolutional networks for large-scale image recognition. *arXiv preprint arXiv:1409.1556*, 2014.

[37] Licheng Jiao, Fan Zhang, Fang Liu, Shuyuan Yang, Lingling Li, Zhixi Feng, and Rong Qu. A survey of deep learning-based object detection. *IEEE access*, 7:128837–128868, 2019.

[38] Shervin Minaee, Yuri Boykov, Fatih Porikli, Antonio Plaza, Nasser Kehtarnavaz, and Demetri Terzopoulos. Image segmentation using deep learning: A survey. *IEEE transactions on pattern analysis and machine intelligence*, 44(7):3523–3542, 2021.

[39] Jie Hu, Li Shen, and Gang Sun. Squeeze-and-excitation networks. In *Proceedings of the IEEE conference on computer vision and pattern recognition*, pages 7132–7141, 2018.

[40] Anil Kag and Venkatesh Saligrama. Condensing cnns with partial differential equations. In *Proceedings of the IEEE/CVF Conference on Computer Vision and Pattern Recognition*, pages 610–619, 2022.

[41] Yifan Sun, Linan Zhang, and Hayden Schaeffer. Neupde: Neural network based ordinary and partial differential equations for modeling time-dependent data. In *Mathematical and Scientific Machine Learning*, pages 352–372. PMLR, 2020.

[42] Ricky TQ Chen, Yulia Rubanova, Jesse Bettencourt, and David K Duvenaud. Neural ordinary differential equations. *Advances in neural information processing systems*, 31, 2018.

[43] Xiaohan Ding, Xiangyu Zhang, Jungong Han, and Guiguang Ding. Scaling up your kernels to 31x31: Revisiting large kernel design in cnns. In *Proceedings of the IEEE/CVF conference on computer vision and pattern recognition*, pages 11963–11975, 2022.

[44] Alexey Dosovitskiy, Lucas Beyer, Alexander Kolesnikov, Dirk Weissenborn, Xiaohua Zhai, Thomas Unterthiner, Mostafa Dehghani, Matthias Minderer, Georg Heigold, Sylvain Gelly, et al. An image is worth 16x16 words: Transformers for image recognition at scale. *arXiv preprint arXiv:2010.11929*, 2020.

[45] Sinong Wang, Belinda Z Li, Madian Khabsa, Han Fang, and Hao Ma. Linformer: Self-attention with linear complexity. *arXiv preprint arXiv:2006.04768*, 2020.

[46] Ze Liu, Yutong Lin, Yue Cao, Han Hu, Yixuan Wei, Zheng Zhang, Stephen Lin, and Baining Guo. Swin transformer: Hierarchical vision transformer using shifted windows. In *Proceedings of the IEEE/CVF international conference on computer vision*, pages 10012–10022, 2021.

[47] Xiaoyi Dong, Jianmin Bao, Dongdong Chen, Weiming Zhang, Nenghai Yu, Lu Yuan, Dong Chen, and Baining Guo. Cswin transformer: A general vision transformer backbone with cross-shaped windows. In *Proceedings of the IEEE/CVF Conference on Computer Vision and Pattern Recognition*, pages 12124–12134, 2022.

[48] Junting Pan, Adrian Bulat, Fuwen Tan, Xiatian Zhu, Lukasz Dudziak, Hongsheng Li, Georgios Tzimiropoulos, and Brais Martinez. Edgevits: Competing light-weight cnns on mobile devices with vision transformers. In *European Conference on Computer Vision*, pages 294–311. Springer, 2022.

[49] Ali Hatamizadeh, Hongxu Yin, Greg Heinrich, Jan Kautz, and Pavlo Molchanov. Global context vision transformers. In *International Conference on Machine Learning*, pages 12633–12646. PMLR, 2023.

[50] Axel Sauer, Tero Karras, Samuli Laine, Andreas Geiger, and Timo Aila. Stylegan-t: Unlocking the power of gans for fast large-scale text-to-image synthesis. *arXiv preprint arXiv:2301.09515*, 2023.

[51] Jiahui Yu, Yuanzhong Xu, Jing Yu Koh, Thang Luong, Gunjan Baid, Zirui Wang, Vijay Vasudevan, Alexander Ku, Yinfei Yang, Burcu Karagol Ayan, et al. Scaling autoregressive models for content-rich text-to-image generation. *arXiv preprint arXiv:2206.10789*, 2022.

[52] Oran Gafni, Adam Polyak, Oron Ashual, Shelly Sheynin, Devi Parikh, and Yaniv Taigman. Make-a-scene: Scene-based text-to-image generation with human priors. In *European Conference on Computer Vision*, pages 89–106. Springer, 2022.

[53] Xiaoliang Dai, Ji Hou, Chih-Yao Ma, Sam Tsai, Jialiang Wang, Rui Wang, Peizhao Zhang, Simon Vandenhende, Xiaofang Wang, Abhimanyu Dubey, et al. Emu: Enhancing image generation models using photogenic needles in a haystack. *arXiv preprint arXiv:2309.15807*, 2023.

[54] Jascha Sohl-Dickstein, Eric Weiss, Niru Maheswaranathan, and Surya Ganguli. Deep unsupervised learning using nonequilibrium thermodynamics. In *International Conference on Machine Learning*, pages 2256–2265. PMLR, 2015.

[55] Yang Song and Stefano Ermon. Generative modeling by estimating gradients of the data distribution. *Advances in neural information processing systems*, 32, 2019.

[56] Susung Hong, Gyuseong Lee, Wooseok Jang, and Seungryong Kim. Improving sample quality of diffusion models using self-attention guidance. In *Proceedings of the IEEE/CVF International Conference on Computer Vision*, pages 7462–7471, 2023.

[57] Jiatao Gu, Shuangfei Zhai, Yizhe Zhang, Joshua M Susskind, and Navdeep Jaitly. Matryoshka diffusion models. In *The Twelfth International Conference on Learning Representations*, 2023.

[58] Shoufa Chen, Mengmeng Xu, Jiawei Ren, Yuren Cong, Sen He, Yanping Xie, Animesh Sinha, Ping Luo, Tao Xiang, and Juan-Manuel Perez-Rua. Gentron: Delving deep into diffusion transformers for image and video generation. *arXiv preprint arXiv:2312.04557*, 2023.

[59] William Peebles and Saining Xie. Scalable diffusion models with transformers. In *Proceedings of the IEEE/CVF International Conference on Computer Vision*, pages 4195–4205, 2023.

[60] Tero Karras, Miika Aittala, Jaakko Lehtinen, Janne Hellsten, Timo Aila, and Samuli Laine. Analyzing and improving the training dynamics of diffusion models. *arXiv preprint arXiv:2312.02696*, 2023.

[61] Ali Hatamizadeh, Jiaming Song, Guilin Liu, Jan Kautz, and Arash Vahdat. Diffit: Diffusion vision transformers for image generation. *arXiv preprint arXiv:2312.02139*, 2023.

[62] Zhida Feng, Zhenyu Zhang, Xintong Yu, Yewei Fang, Lanxin Li, Xuyi Chen, Yuxiang Lu, Jiaxiang Liu, Weichong Yin, Shikun Feng, et al. Ernie-vilg 2.0: Improving text-to-image diffusion model with knowledge-enhanced mixture-of-denoising-experts. In *Proceedings of the IEEE/CVF Conference on Computer Vision and Pattern Recognition*, pages 10135–10145, 2023.

[63] Zeyue Xue, Guanglu Song, Qiushan Guo, Boxiao Liu, Zhuofan Zong, Yu Liu, and Ping Luo. Raphael: Text-to-image generation via large mixture of diffusion paths. *Advances in Neural Information Processing Systems*, 36, 2024.

[64] Xinyin Ma, Gongfan Fang, and Xinchao Wang. Deepcache: Accelerating diffusion models for free. *arXiv preprint arXiv:2312.00858*, 2023.

[65] Muyang Li, Tianle Cai, Jiaxin Cao, Qinsheng Zhang, Han Cai, Junjie Bai, Yangqing Jia, Ming-Yu Liu, Kai Li, and Song Han. Distrifusion: Distributed parallel inference for high-resolution diffusion models. In *Proceedings of the IEEE/CVF Conference on Computer Vision and Pattern Recognition (CVPR)*, 2024.

[66] Felix Wimbauer, Bichen Wu, Edgar Schoenfeld, Xiaoliang Dai, Ji Hou, Zijian He, Artsiom Sanakoyeu, Peizhao Zhang, Sam Tsai, Jonas Kohler, et al. Cache me if you can: Accelerating diffusion models through block caching. *arXiv preprint arXiv:2312.03209*, 2023.

[67] Ryan Webster, Julien Rabin, Loic Simon, and Frederic Jurie. On the de-duplication of laion-2b. *arXiv preprint arXiv:2303.12733*, 2023.

[68] Aaron Gokaslan, A Feder Cooper, Jasmine Collins, Landan Seguin, Austin Jacobson, Mihir Patel, Jonathan Frankle, Cory Stephenson, and Volodymyr Kuleshov. Commoncanvas: An open diffusion model trained with creative-commons images. *arXiv preprint arXiv:2310.16825*, 2023.

[69] Junsong Chen, Jincheng Yu, Chongjian Ge, Lewei Yao, Enze Xie, Yue Wu, Zhongdao Wang, James Kwok, Ping Luo, Huchuan Lu, and Zhenguo Li. Pixart-α: Fast training of diffusion transformer for photorealistic text-to-image synthesis, 2023.

[70] Pablo Pernias, Dominic Rampas, Mats Leon Richter, Christopher Pal, and Marc Aubreville. Würstchen: An efficient architecture for large-scale text-to-image diffusion models. In *The Twelfth International Conference on Learning Representations*, 2023.

[71] Junsong Chen, Chongjian Ge, Enze Xie, Yue Wu, Lewei Yao, Xiaozhe Ren, Zhongdao Wang, Ping Luo, Huchuan Lu, and Zhenguo Li. Pixart-\sigma: Weak-to-strong training of diffusion transformer for 4k text-to-image generation. *arXiv preprint arXiv:2403.04692*, 2024.

[72] Olga Russakovsky, Jia Deng, Hao Su, Jonathan Krause, Sanjeev Satheesh, Sean Ma, Zhiheng Huang, Andrej Karpathy, Aditya Khosla, Michael Bernstein, et al. Imagenet large scale visual recognition challenge. *International journal of computer vision*, 115:211–252, 2015.

[73] Mingxing Tan and Quoc Le. Efficientnet: Rethinking model scaling for convolutional neural networks. In *International conference on machine learning*, pages 6105–6114. PMLR, 2019.

[74] Zhuang Liu, Hanzi Mao, Chao-Yuan Wu, Christoph Feichtenhofer, Trevor Darrell, and Saining Xie. A convnet for the 2020s. In *Proceedings of the IEEE/CVF Conference on Computer Vision and Pattern Recognition (CVPR)*, pages 11976–11986, June 2022.

[75] Andrew Howard, Mark Sandler, Grace Chu, Liang-Chieh Chen, Bo Chen, Mingxing Tan, Weijun Wang, Yukun Zhu, Ruoming Pang, Vijay Vasudevan, et al. Searching for mobilenetv3. In *Proceedings of the IEEE/CVF international conference on computer vision*, pages 1314–1324, 2019.

[76] Dan Hendrycks and Kevin Gimpel. Gaussian error linear units (gelus). *arXiv preprint arXiv:1606.08415*, 2016.

[77] Mostafa Dehghani, Josip Djolonga, Basil Mustafa, Piotr Padlewski, Jonathan Heek, Justin Gilmer, Andreas Peter Steiner, Mathilde Caron, Robert Geirhos, Ibrahim Alabdulmohsin, et al. Scaling vision transformers to 22 billion parameters. In *International Conference on Machine Learning*, pages 7480–7512. PMLR, 2023.

[78] Hugo Touvron, Matthieu Cord, Alaaeldin El-Nouby, Jakob Verbeek, and Hervé Jégou. Three things everyone should know about vision transformers, 2022.

[79] Weifeng Lin, Ziheng Wu, Jiayu Chen, Jun Huang, and Lianwen Jin. Scale-aware modulation meet transformer, 2023.

[80] Lei Zhu, Xinjiang Wang, Zhanghan Ke, Wayne Zhang, and Rynson Lau. Biformer: Vision transformer with bi-level routing attention. *Proceedings of the IEEE/CVF Conference on Computer Vision and Pattern Recognition (CVPR)*, 2023.

[81] Qihang Fan, Huaibo Huang, Mingrui Chen, Hongmin Liu, and Ran He. Rmt: Retentive networks meet vision transformers. In *CVPR*, 2024.

[82] Siyuan Li, Zedong Wang, Zicheng Liu, Cheng Tan, Haitao Lin, Di Wu, Zhiyuan Chen, Jiangbin Zheng, and Stan Z. Li. Moganet: Multi-order gated aggregation network. In *International Conference on Learning Representations*, 2024.

[83] Diederik P Kingma and Max Welling. Auto-encoding variational bayes. *arXiv preprint arXiv:1312.6114*, 2013.

[84] Danilo Jimenez Rezende, Shakir Mohamed, and Daan Wierstra. Stochastic backpropagation and approximate inference in deep generative models. In *International conference on machine learning*, pages 1278–1286. PMLR, 2014.

[85] Hyung Won Chung, Le Hou, Shayne Longpre, Barret Zoph, Yi Tay, William Fedus, Yunxuan Li, Xuezhi Wang, Mostafa Dehghani, Siddhartha Brahma, et al. Scaling instruction-finetuned language models. *Journal of Machine Learning Research*, 25(70):1–53, 2024.

[86] Fan Bao, Shen Nie, Kaiwen Xue, Yue Cao, Chongxuan Li, Hang Su, and Jun Zhu. All are worth words: A vit backbone for diffusion models. In *Proceedings of the IEEE/CVF Conference on Computer Vision and Pattern Recognition*, pages 22669–22679, 2023.

[87] Jianlin Su, Murtadha Ahmed, Yu Lu, Shengfeng Pan, Wen Bo, and Yunfeng Liu. Roformer: Enhanced transformer with rotary position embedding. *Neurocomputing*, 568:127063, 2024.

[88] Biao Zhang and Rico Sennrich. Root mean square layer normalization. *Advances in Neural Information Processing Systems*, 32, 2019.

[89] Ilya Loshchilov and Frank Hutter. Decoupled weight decay regularization. In *International Conference on Learning Representations*, 2019.

[90] Patrick Esser, Sumith Kulal, Andreas Blattmann, Rahim Entezari, Jonas Müller, Harry Saini, Yam Levi, Dominik Lorenz, Axel Sauer, Frederic Boesel, et al. Scaling rectified flow transformers for high-resolution image synthesis. *arXiv preprint arXiv:2403.03206*, 2024.

[91] Wenhai Wang, Enze Xie, Xiang Li, Deng-Ping Fan, Kaitao Song, Ding Liang, Tong Lu, Ping Luo, and Ling Shao. Pvt v2: Improved baselines with pyramid vision transformer. *Computational Visual Media*, 8(3):415–424, March 2022.

[92] Chenglin Yang, Siyuan Qiao, Qihang Yu, Xiaoding Yuan, Yukun Zhu, Alan Yuille, Hartwig Adam, and Liang-Chieh Chen. MOAT: Alternating mobile convolution and attention brings strong vision models. In *The Eleventh International Conference on Learning Representations*, 2023.

[93] Han Cai, Chuang Gan, and Song Han. Efficientvit: Enhanced linear attention for high-resolution low-computation visual recognition. *arXiv preprint arXiv:2205.14756*, 2022.

[94] Tal Ridnik, Emanuel Ben-Baruch, Asaf Noy, and Lihi Zelnik-Manor. Imagenet-21k pretraining for the masses, 2021.

[95] Martin Heusel, Hubert Ramsauer, Thomas Unterthiner, Bernhard Nessler, and Sepp Hochreiter. Gans trained by a two time-scale update rule converge to a local nash equilibrium. *Advances in neural information processing systems*, 30, 2017.

[96] Jonathan Ho and Tim Salimans. Classifier-free diffusion guidance. *arXiv preprint arXiv:2207.12598*, 2022.

[97] Dhruba Ghosh, Hanna Hajishirzi, and Ludwig Schmidt. Geneval: An object-focused framework for evaluating text-to-image alignment, 2023.

[98] Ekin Dogus Cubuk, Barret Zoph, Jon Shlens, and Quoc Le. Randaugment: Practical automated data augmentation with a reduced search space. In H. Larochelle, M. Ranzato, R. Hadsell, M.F. Balcan, and H. Lin, editors, *Advances in Neural Information Processing Systems*, volume 33, pages 18613–18624. Curran Associates, Inc., 2020.

[99] Hongyi Zhang, Moustapha Cisse, Yann N. Dauphin, and David Lopez-Paz. mixup: Beyond empirical risk minimization. In *International Conference on Learning Representations*, 2018.

[100] Ross Wightman. Pytorch image models. https://github.com/rwightman/pytorch-image-models, 2019.

[101] Andy Brock, Soham De, Samuel L Smith, and Karen Simonyan. High-performance large-scale image recognition without normalization. In *International Conference on Machine Learning*, pages 1059–1071. PMLR, 2021.

[102] Donghyun Kim, Byeongho Heo, and Dongyoon Han. Densenets reloaded: Paradigm shift beyond resnets and vits, 2024.

[103] Hugo Touvron, Matthieu Cord, Matthijs Douze, Francisco Massa, Alexandre Sablayrolles, and Hervé Jégou. Training data-efficient image transformers & distillation through attention. In *International conference on machine learning*, pages 10347–10357. PMLR, 2021.

[104] Bolei Zhou, Hang Zhao, Xavier Puig, Sanja Fidler, Adela Barriuso, and Antonio Torralba. Scene parsing through ade20k dataset. In *2017 IEEE Conference on Computer Vision and Pattern Recognition (CVPR)*, pages 5122–5130, 2017.

[105] MMSegmentation Contributors. MMSegmentation: Openmmlab semantic segmentation toolbox and benchmark. https://github.com/open-mmlab/mmsegmentation, 2020.

[106] Tete Xiao, Yingcheng Liu, Bolei Zhou, Yuning Jiang, and Jian Sun. Unified perceptual parsing for scene understanding. In *European Conference on Computer Vision*. Springer, 2018.

[107] Junnan Li, Dongxu Li, Silvio Savarese, and Steven Hoi. BLIP-2: Bootstrapping language-image pre-training with frozen image encoders and large language models. In Andreas Krause, Emma Brunskill, Kyunghyun Cho, Barbara Engelhardt, Sivan Sabato, and Jonathan Scarlett, editors, *Proceedings of the 40th International Conference on Machine Learning*, volume 202 of *Proceedings of Machine Learning Research*, pages 19730–19742. PMLR, 23–29 Jul 2023.

A Appendix

A.1 Image Recognition Architecture Details

We describe the three AsCAN variants (tiny, base, and large) used in the experiments (see Sec. 4.1) in the Tab. 6. We follow earlier works [31] to scale the tiny variant discussed in Sec. 3.1. Note that the stem consists of two convolutional layers that downsample the input to half the spatial resolution. The classifier stage projects the final feature map to the corresponding embedding size and performs adaptive average pooling to reduce the spatial dimensions to 1×1, in order to apply a feed-forward layer that acts as classifier head on top of these pooled features. Our convolution blocks use the batch-norm as the normalization layer while the transformer blocks leverage the layer-norm as the normalization layer. We also learn the relative positional embeddings in our attention mechanism similar to earlier works [31, 32, 46].

Table 6: **Architecture Details.** We provide detailed configuration of the three variants of the AsCAN proposed in this work, namely, tiny, base, and large. As per our method section, we use FusedMBConv (`C`) as the convolution block and Vanilla Transformer (`T`) as the transformer block. We refer the reader to the Fig. 2 for their detailed description and schematic of these building blocks. We use K to denote the number of classes. Note that we hide the activation and normalization layers in the blocks. We use GeLU activation and batch-normalization in the Stem and the classifier stages.

Stage	Tiny	Base	Large
S0: Stem	Conv 3×3, Channels 64, Stride 2 Conv 3×3, Channels 64, Stride 1	Conv 3×3, Channels 64, Stride 2 Conv 3×3, Channels 64, Stride 1	Conv 3×3, Channels 128, Stride 2 Conv 3×3, Channels 128, Stride 1
S1: Only-Conv	`C`, Channels 96, Stride 2 `C`, Channels 96, Stride 1	`C`, Channels 96, Stride 2 `C`, Channels 96, Stride 1	`C`, Channels 128, Stride 2 `C`, Channels 128, Stride 1
S2: Mix	`C`, Channels 192, Stride 2 `C`, Channels 192, Stride 1 `C`, Channels 192, Stride 1 `T`, Channels 192, Stride 1	(`C`, Channels 192, Stride 2) $\times 1$ (`C`, Channels 192, Stride 1) $\times 3$ (`T`, Channels 192, Stride 1) $\times 2$	(`C`, Channels 256, Stride 2) $\times 1$ (`C`, Channels 256, Stride 1) $\times 3$ (`T`, Channels 256, Stride 1) $\times 2$
S3: Mix	`C`, Channels 384, Stride 2 `C`, Channels 384, Stride 1 `T`, Channels 384, Stride 1 `T`, Channels 384, Stride 1	(`C`, Channels 384, Stride 2) $\times 1$ (`C`, Channels 384, Stride 1) $\times 6$ (`T`, Channels 384, Stride 1) $\times 7$	(`C`, Channels 512, Stride 2) $\times 1$ (`C`, Channels 512, Stride 1) $\times 6$ (`T`, Channels 512, Stride 1) $\times 7$
S4: Mix	`C`, Channels 768, Stride 2 `T`, Channels 768, Stride 1 `T`, Channels 768, Stride 1 `T`, Channels 768, Stride 1	`C`, Channels 768, Stride 2 `T`, Channels 768, Stride 1 `T`, Channels 768, Stride 1 `T`, Channels 768, Stride 1	`C`, Channels 1024, Stride 2 `T`, Channels 1024, Stride 1 `T`, Channels 1024, Stride 1 `T`, Channels 1024, Stride 1
S5: Classifier	Conv 1×1, Channels 512 Adaptive Avg Pool Feed-Forward $512\times$ K	Conv 1×1, Channels 768 Adaptive Avg Pool Feed-Forward $768\times$ K	Conv 1×1, Channels 1024 Adaptive Avg Pool Feed-Forward $1024\times$ K

A.2 ImageNet Classification (Training Procedure & Hyper-parameters)

We follow the same training strategy for our ImageNet experiments in Sec. 3.1 and Sec. 4.1. We report the top-1 accuracy on the single center crop image. For training ImageNet-1K models with 224×224 resolution, we use the AdamW optimizer with a peak learning rate of $3e-3$ for 300 epochs. We use a batch size of 4096 images during this training period. We follow a cosine schedule for decaying the learning rate to the minimum learning rate of $5e-6$. We also perform a learning rate warm-up to avoid instabilities during the training. We follow a 20 epoch warm-up schedule with an initial learning rate of $5e-7$ that gets warmed up to the peak learning rate.

For all our experiments, we use standard data augmentation strategies. We use RandAugment [98] with parameters $(2, 15)$, MixUp [99] with $\alpha = 0.8$, color jittering with 0.4 as the weight, and label smoothing with 0.1 as the smoothing parameter. We also use 0.05 value for the weight decay regularization and perform an exponential model averaging with a decay value of 0.9999. In addition, we adopt gradient clipping with a gradient norm of 1.0 to avoid instabilities during the training of such large models. We also enable stochastic depth for regularization. We use the stochastic depth of $0.3/0.4/0.5$ for the three variants in our experiments.

A.2.1 ImageNet-1K

We benchmark various existing architectures on two accelerators (NVIDIA A100 and V100 GPUs) with different batch sizes to evaluate the inference speed of a single forward pass. Additionally, we train the three AsCANvariants with the training procedure described in earlier sections. We show the full results corresponding to the Fig. 3 in the Tab. 7. We also include inference memory consumed by various recent works in Tab. 8.

A.2.2 Ablations on Architecture Configuration

One of the AsCAN design principles include preferring `C` blocks over `T` blocks in a stage. We demonstrated various architecture configurations using this design choice in Tab. 2. For completeness, we reverse this design choice and prefer `T` blocks over `C` blocks in a stage. We show these configurations in Tab. 9. Using **T** block in stem / early layers result in lower throughput. Further, the performance of configurations with **T** before **C** yields lower accuracy vs throughput trade-off.

A.2.3 ImageNet-21K

We also study the effects of pre-training the AsCAN family on larger datasets such as ImageNet-21K [72]. Similar to earlier works, we pre-train our models on the ImageNet-21K dataset. We use the pre-processed version of this dataset for ease of usage [94]. Following previous works [11, 31], we train the AsCAN model for 90 epochs on the ImageNet-21K dataset and fine-tune these weights on the ImageNet-1K classification task. Similar to the ImageNet-1K experiments, we use RandAugment [98] with parameters $(2, 5)$, MixUp [99] with $\alpha = 0.2$, color jittering with 0.4 as the weight and label smoothing with 0.01 as the smoothing parameter. We also use 0.01 value for the weight decay regularization. Additionally, we perform an exponential model averaging with a decay value of 0.9999 and gradient clipping with a gradient norm of 1.0 to avoid instabilities during training such large models. We also enable stochastic depth for regularization. We use the stochastic depth of $0.4/0.5/0.6$ for the three variants in our experiments.

We report the performance in Tab. 10, where we observe similar top-1 accuracy as the other baselines while achieving much better inference throughput. This trend is similar to the one we observed in Sec. 4.1 when these models trained only on the ImageNet-1K dataset without any pre-training on the ImageNet-21K dataset.

A.3 ADE20K Semantic Segmentation

Dataset Details. ADE20K [104] is a popular scene-parsing dataset used to evaluate the semantic segmentation performance. It consists of 20K train and 2K validation images over 150 fine-grained semantic categories. Images are resized and cropped to 512×512 resolution for training.

Training Procedure & Hyper-parameters. We base our semantic segmentation experiments on the widely used and publicly available mmsegmentation library [105]. We use the UPerNet [106] as our semantic segmentation architecture wherein different hybrid architectures are used as the backbones to extract the spatial feature maps. We extract the spatial feature maps at stages S2, S3, and S4, and forward these feature maps to the semantic segmentation network. All three AsCAN variants (tiny, base, large) have been initialized with the weights pre-trained on the ImageNet-1K task with 224×224 resolution. Training is performed in 512×512 resolution. Similar to FasterViT [32], we follow a similar schedule for training these segmentation models with an AdamW optimizer with a learning rate of $1e - 4$, and a weight decay of 0.05. We use a batch size of 16 on 8 A100 GPUs. We also use stochastic depth similar to ImageNet training for controlling overfitting during these experiments.

Experimental Setup. We train UperNet [106] as segmentation architecture on the ADE20K dataset. We use the proposed AsCAN as the backbone pre-trained on the ImageNet-1K dataset. We use the AdamW optimizer [89] with learning rate $1e - 4$ and weight decay 0.05. Following earlier works [32, 74], we train the models for 160K iterations using the mmsegmentation library [105]. We train these networks on 8 NVIDIA A100 GPUs using 16 as the batch size. We compute the various inference statistics with 512×512 as the image resolution.

Experimental Results. We compare the performance of various backbones in Tab. 11. It shows that the proposed backbone achieves competitive mIoU while achieving nearly $1.5\times$ faster inference latency compared to the baselines, measured using the frames per second metrics. This fact can be observed across different scaling of the backbones. For instance, the Swin-T backbone achieves latency of 44FPS while AsCAN-T achieves 64FPS as the latency with similar mIoU. Thus, our models achieve a similar performance-*vs.*-latency trend at the downstream semantic segmentation task as the classification benchmark.

A.4 T2I Dataset Details

We curate our training dataset with careful filtration on diverse data sources using first-party and licensed datasets. We depict this entire process in Fig. 6. We start by collating all these data sources to create a stream of images and if available, relevant text captions. Next stage, we add a series of filters to improve the quality of the selected images (resolution, de-duplication, aesthetic score, nsfw filtering, *etc.*). Since this data mostly contains very short descriptions or almost non-existent descriptions of the image, we unify the captioning process using an image captioning model. We collect a subset of 200K data for human annotations, where we ask the annotators to add details such as the `<angle shot of the image>`, `<image background information>`, `<human attributes>`, *etc.* We use this labeled data to fine-tune a BLIP2 [107] model which is used to generate long captions similar to this format.

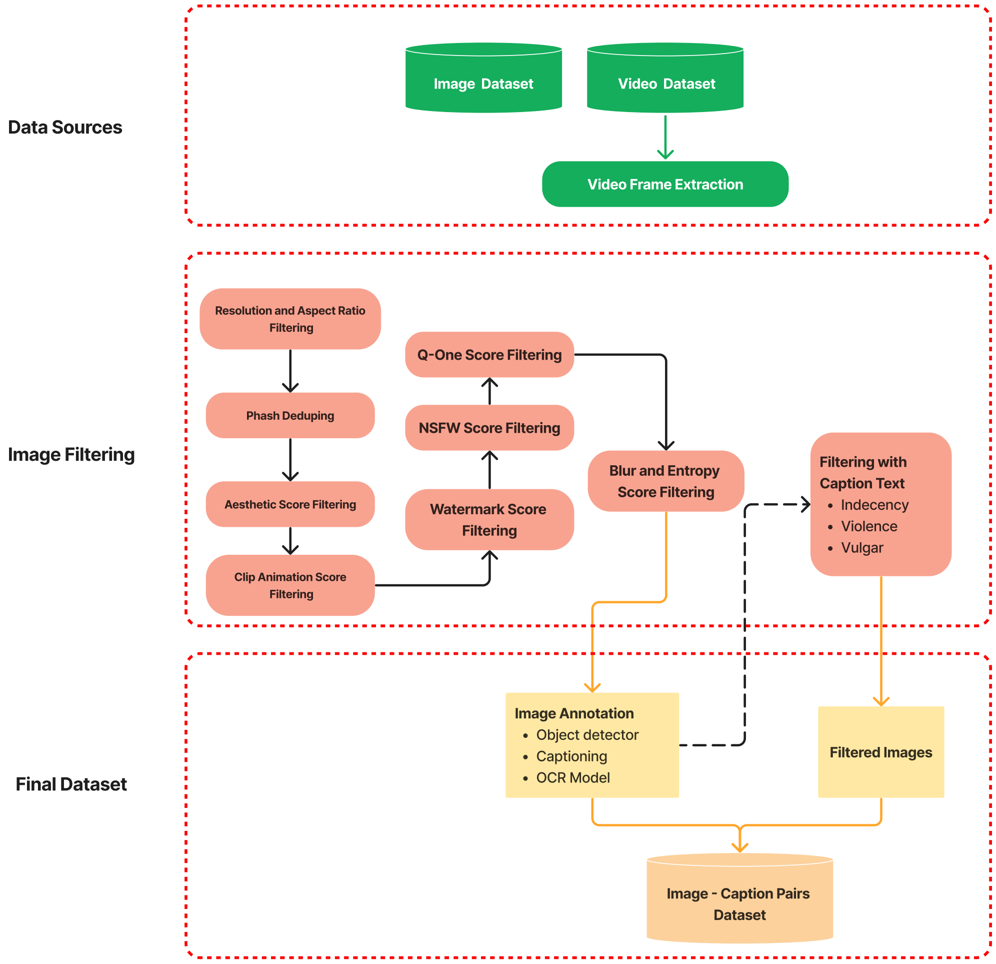

Figure 6: **Curation Pipeline for the T2I Dataset.** We show various stages involved in the creation of our T2I dataset.

A.5 T2I Evaluation Details.

A.5.1 Resource Usage

We compare the resource usage of various existing methods with our proposed T2I model. Tab. 12 shows the parameter count of the model, training compute cost, and the inference cost per image generation.

A.5.2 Evaluation on Internal Data

We evaluate our models against various baselines on two internally captioned datasets (Set-A-10K and Set-B-10K). We draw these datasets from our validation set. We compute the FID between the generated 10K images against the reference images in Tab. 5. This table also shows that fast training pipelines like PixArt-α and PixArt-Σ suffer considerably when evaluated on real-world images compared to models like SDXL and Ours. We also point out that SDXL has been trained with a considerably larger dataset compared to ours and uses much more computational resources.

A.6 Hyper-parameter Setup for Text-to-Image Generation

Since full-scale text-to-image generation task is a computationally expensive task, it becomes crucial that we choose appropriate hyper-parameters and initialization of the model before training it on the entire dataset. Thus, we choose a proxy task that can be run on a small scale and guide us in the suitable training configurations.

ImageNet-1K T2I Generation Task. We resort to the ImageNet-1K dataset since it contains a variety of objects (1000 objects) in different settings. Earlier works such as Pixart-α, train their transformer architecture on the ImageNet-1K class-conditional generation tasks, wherein they incorporate the text condition via a cross-attention mechanism. This process requires the model to forget the class condition and adapt to the text condition. In this work, along the lines of [90], we simply convert the ImageNet-1K classification dataset to Text-to-Image dataset by adding the text corresponding to the `<class name>`, with the template "a photo of a `<class name>`". Specifically, the dataset provides various different names corresponding to each class, we pick up one at random during training to learn diverse text mappings. We evaluate the models by computing the FID between the 50K generated images and the reference images from the dataset.

Embedding Pre-Computation. Our T2I model performs diffusion in the latent space. To keep parity between this task and the full training, we also pre-compute the SDXL VAE embeddings of the ImageNet-1K dataset. Similarly, we pre-compute Flan-T5-XXL embeddings for the text condition. This saves training resources since loading VAE and Flan-T5-XXL encoders consumes significant GPU memory as well as non-trivial computation time. Thus, by pre-computing these embeddings, we increase the batch size available for training the UNet model.

Architecture Details. We use similar configuration for the `C` blocks as in the image recognition architecture. All our convolutional operators use 3×3 kernel sizes. The number of output channels in the three `Down` blocks are $\{320, 640, 1280\}$. Since the three `Up` blocks are reflections of the `Down` blocks, their output channels are in the reverse order, *i.e.*, $\{1280, 640, 320\}$. Given that we use the SDXL VAE to convert the $3-$channel RGB-image into $4-$channel latent space, our number of input channels is 4 for the convolution operator in the first `Down` block. The number of attention heads in the three `T` blocks in the three `Down` stages are $\{5, 10, 20\}$. Since our `T` blocks are applied after `C` blocks, the number of output channels of the convolutional blocks along with the number of attention heads, determine the attention dimension for the transformer block. Finally, we compute the time-step and textual embeddings. The time-step integer values are converted to timestep embedding by first converting it into sinusoidal space and then projecting it through two linear layers. We process the textual embeddings using two `T` blocks for adapting the frozen embeddings (dimension 4096) for T2I generation with just one head and the same dimension as the frozen embeddings.

Noise Level Ablation for Different Resolutions. Since our training strategy involves jumping resolutions from $256 \rightarrow 512 \rightarrow 1024$, we ablate on the noise levels at each of these resolutions. We use the DDPM noise scheduler for injecting the noise and the level of noise is controlled by the β_T hyper-parameter. We try four different noise levels $\{0.01, 0.02, 0.03, 0.04\}$, and compute the FID scores. We plot these scores in Fig. 7. We find that at resolution 256, noise level 0.01 produces the best FID score, and at remaining resolutions, noise level 0.02 works the best.

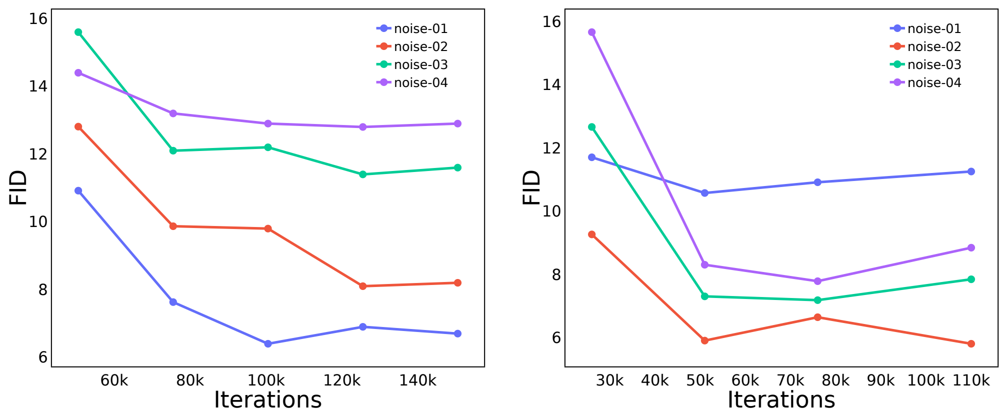

Figure 7: **Noise Level Selection for Different Resolution.** We ablate on the end noise level during the epsilon-prediction for the ImageNet-1k T2I task for the 256×256 (*Left*) and 512×512 (*Right*) resolutions with different learning rate and weight decay parameters. We plot the FID scores against a reference image set from the dataset.

T2I Task Initialization Ablation. We analyze initializing the 256×256 resolution training with and without pre-training from the ImageNet-1K T2I pre-trained model. As shown in Fig. 8, pre-training helps improve the performance of the model compared to training from scratch.

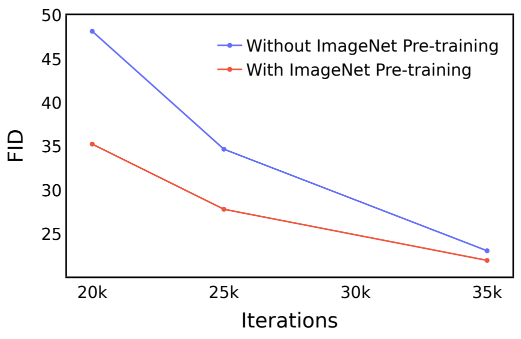

Figure 8: **Comparing T2I** 256×256 **Resolution Training with and w/o Pre-training.** We report the FID score on Set-B-10K for 256×256 resolution training, with and without pre-training from the ImageNet-1k T2I model.

A.7 ImageNet-1K Class Conditional Generation.

We learn a class conditional image generation on the ImageNet-1K dataset with image resolution 256×256. We train a smaller variant of our asymmetric UNet architecture (as in Sec. 3.3.1) with nearly 400M parameters and inject the class condition through the cross-attention mechanism. We train this model using the DDPM scaled linear noise schedule for 1000 time steps. The training is conducted for 1000 epochs with a batch size of 2048. We use AdamW optimizer with $6e-4$ as the learning rate, 0.01 as the weight decay, and $(\beta_1, \beta_2) = (0.9, 0.99)$. We use an $8-$channel VAE to convert the input image space into a latent space for latent diffusion. We compare our results with other class conditional models in Tab. 4. Our asymmetric architecture for this task is similar to the T2I UNet architecture described earlier. To lower down the compute footprint, we reduce the number of channels to $\{160, 320, 640\}$ and reduce the cross-attention dimension from 4096 to 768. We evaluate our model with two configurations and report these two FID scores. In the first configuration, we apply a classifier-free guidance (cfg) scale [96] of 1.78 to generate the class-conditioned images. In the second configuration (sampled cfg), we apply the guidance in the steps $[5, 30]$ with a cfg scale in the increasing range $[1.1, 3.6]$. This sampling procedure is similar to the one proposed in MUSE [23]. We use the Heun [19] discrete scheduler for inference with 30 sampling steps.

A.8 Limitations

We develop hybrid architectures with asymmetric distribution of the convolution and transformer blocks. We show that this design paradigm is generic and applicable to many vision tasks such as image recognition, semantic segmentation, and text-to-image generation. We expect this architecture design to be widely useful for other applications. From the architecture design perspective, our building blocks are not rigid and can be replaced with other efficient alternatives of the chosen `C` and `T` blocks. Currently, we focus on the vanilla attention mechanism, but we can certainly incorporate faster alternatives to quadratic attention without sacrificing any efficiency advantages. Since we demonstrate an application of the asymmetric design to the UNet framework, we list out some limitations of our text-to-image generation model, which is broadly similar to various existing text-to-image models.

- *Extra limbs.* While our model is able to generate limbs for humans and animals very well in most cases. There are instances where we can observe extra limbs in generations. It is unclear if this is due to a poorly learned diffusion process, poor captioning guidance, lack of granular information in image-caption pairs, or just an artifact of the VAE encoder while converting to the latent space.
- *Artifacts in extreme resolutions.* We train our T2I model with multi-aspect ratio bucketing. While it is able to adapt to many different resolutions in a graceful manner, we find that the model generates duplicate patterns in the extremes of the aspect ratio (significantly higher width than height or vice-versa). We believe this is due to the lack of training data in such resolutions.
- While we are much better at avoiding NSFW generations compared to baselines (due to careful curation of the training data), there might be a slight percentage of NSFW content, due to leakage in various filtration processes in the dataset curation. Thus, we incorporate an additional NFSW filter on top of the generation to remove such edge cases.

A.9 Societal Impact

We design the asymmetric architecture and show the advantages it brings in many applications (image recognition, semantic segmentation, and text-to-image generation). Our architecture design targets a better trade-off between efficiency (training/inference latency) while achieving achieving good performance. In itself, the asymmetric design would reduce the amount of resources utilized by deep neural networks used commonly in vision tasks. The downstream applications of this architecture, especially in Text-to-Image generation need to be deployed with care. We expect the community to utilize proper care *w.r.t.* training data as well as the generated output. There needs to be special checks in place while preparing the training data for T2I tasks. We specially add various filters to remove malicious and harmful content from the dataset. Further, even generated images need to be processed with some filtration to remove similar harmful and malicious content.

A.10 Text-to-Image Generation Results.

For visualization purposes, we generate more images with different prompts using our multi-aspect ratio model. We present these images in Fig. 9, 10, and 11. It shows that our model is able to generate a wide range of images, both very realistic as well as stylistic images. In addition, it is able to grasp various concepts and compositions.

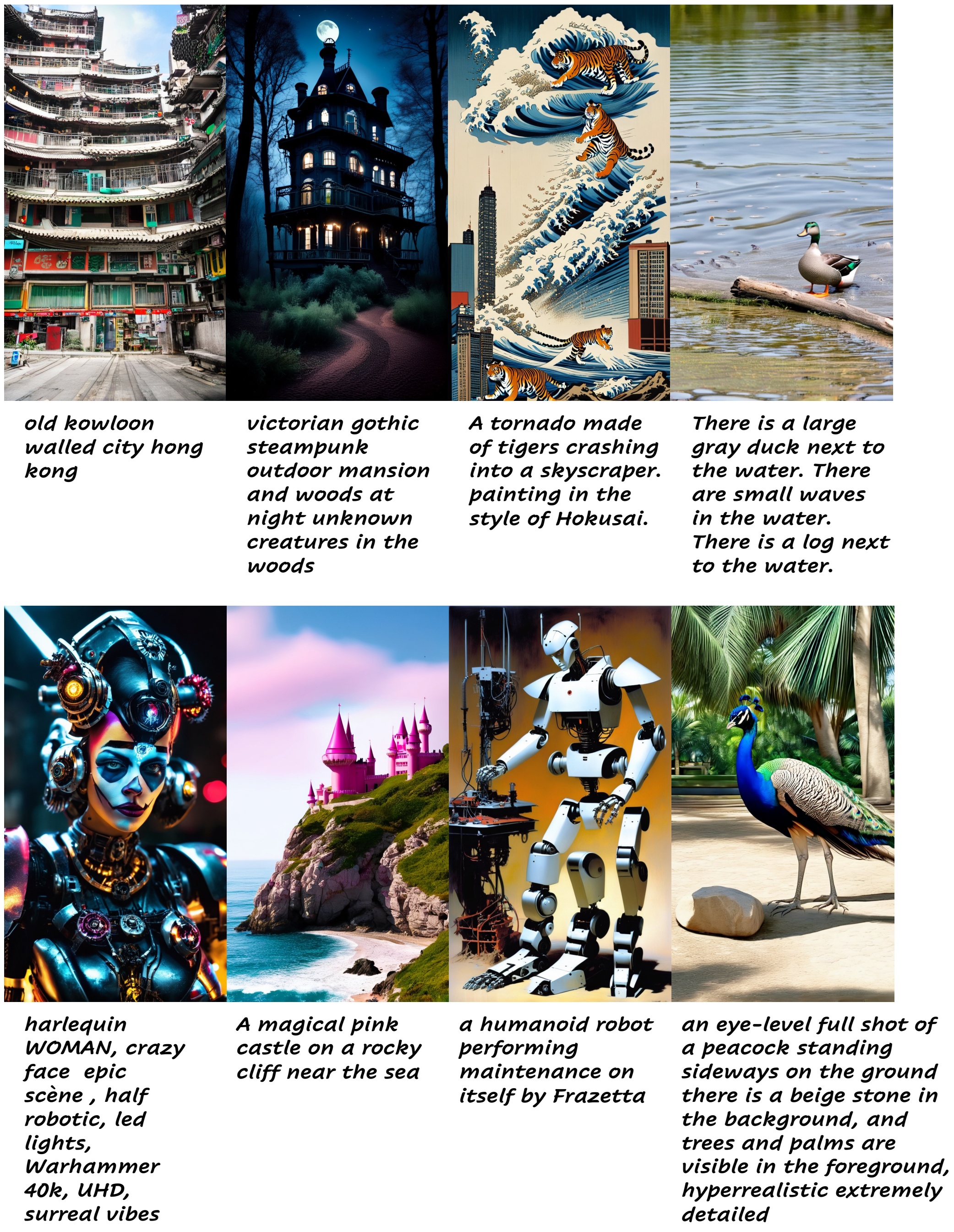
old kowloon walled city hong kong
victorian gothic steampunk outdoor mansion and woods at night unknown creatures in the woods
A tornado made of tigers crashing into a skyscraper. painting in the style of Hokusai.
There is a large gray duck next to the water. There are small waves in the water. There is a log next to the water.
harlequin WOMAN, crazy face epic scène , half robotic, led lights, Warhammer 40k, UHD, surreal vibes
A magical pink castle on a rocky cliff near the sea
a humanoid robot performing maintenance on itself by Frazetta
an eye-level full shot of a peacock standing sideways on the ground there is a beige stone in the background, and trees and palms are visible in the foreground, hyperrealistic extremely detailed

Figure 9: Example text-to-image generation results.

Table 7: **Results on ImageNet-1K [72] for Classification Task.** We compare the performance of our asymmetric architectures, AsCAN, against baselines. We report the inference latency as the throughput (images per second) that is measured by inferring images with batch size as B in half-precision, *i.e.*, fp16, on an A100 GPU using torch-compile and benchmark utility from timm library [100]. A similar procedure (without torch-compile) is followed to obtain the throughput on the V100 GPU.

	Architecture	**Resolution**	**Params**	**MACs**	**Throughput (images/s) Batch (B)**					**Top-1 Accuracy**
					A100			**V100**		
					B=1	**B=16**	**B=64**	**B=1**	**B=16**	
ConvNet	EfficientNet-B6 [73]	528	43M	19.0G	88	529	589	27	205	84.0%
	EfficientNet-B7 [73]	600	66M	37.0G	72	321	350	24	124	84.3%
	NFNet-F0 [101]	256	72M	12.4G	199	2470	3348	47	813	83.6%
	NFNet-F1 [101]	320	132M	35.5G	106	998	1192	26	48	84.7%
	EfficientNetV2-S [1]	384	24M	8.8G	112	1884	2744	34	561	83.9%
	EfficientNetV2-M [1]	480	55M	24.0G	84	918	1094	26	329	85.1%
	ConvNeXt-S [74]	224	50M	8.7G	174	2291	2889	56	836	83.1%
	ConvNeXt-B [74]	224	89M	15.4G	167	1760	2073	58	619	83.8%
	ConvNeXt-L [74]	224	198M	34.4G	168	1045	1127	58	362	84.3%
	RDNet-S [102]	224	50M	8.7G	102	1782	2761	53	780	83.7%
	RDNet-B [102]	224	87M	15.4G	80	1578	1891	48	589	84.4%
	RDNet-L [102]	224	186M	34.7G	78	640	990	32	290	84.8%
ViT	ViT-B/16 [10]	384	86M	55.4G	212	1006	1266	104	86	77.9%
	ViT-B/32 [10]	384	307M	190.7G	112	893	924	54	27	76.5%
	DeiT-B [103]	384	86M	55.4G	189	1058	1192	130	488	83.1%
	Swin-S [46]	224	50M	8.7G	50	841	2221	34	436	83.0%
	Swin-B [46]	384	88M	47.0G	51	458	486	20	85	84.5%
Hybrid	PVTv2-B3[91]	224	45M	7G	49	933	3782	33	548	83.2%
	PVTv2-B5[91]	224	82M	11.8G	32	511	2112	17	291	83.8%
	EfficientViT-B2[93]	224	24M	1.6G	142	2171	5132	48	782	82.1%
	EfficientViT-B3[93]	224	49M	4G	114	1882	2860	32	552	83.5%
	MOAT-2[92]	224	73M	17.2G	132	1367	2087	38	424	84.7%
	MOAT-3[92]	224	190M	44.9G	70	805	962	21	246	85.3%
	SMT-S[79]	224	21M	4.7G	38	566	2211	43	348	83.7%
	SMT-B[79]	224	32M	7.7G	27	388	1412	14	243	84.3%
	MogaNet-L [82]	224	83M	15.9G	34	523	882	24	290	84.7%
	MogaNet-XL [82]	224	181M	34.5G	32	471	576	19	210	85.1%
	BiFormer-S [80]	224	26M	4.5G	45	937	2139	36	595	83.8%
	BiFormer-B [80]	224	57M	9.8G	50	840	1439	28	440	84.3%
	RMT-S [81]	224	27M	4.5G	46	790	2439	38	480	84.1%
	CoAtNet-0 [11]	224	25M	4.2G	214	3537	5221	61	976	81.6%
	CoAtNet-1 [11]	224	42M	8.4G	141	2221	2907	45	629	83.3%
	CoAtNet-2 [11]	224	75M	15.7G	133	1718	2040	38	540	84.1%
	CoAtNet-3 [11]	224	168M	34.7G	132	1085	1105	37	388	84.5%
	MaxViT-T [31]	224	31M	5.6G	73	1098	2756	23	357	83.62%
	MaxViT-S [31]	224	69M	11.7G	70	1019	1775	24	243	84.45%
	MaxViT-B [31]	224	120M	23.4G	34	507	1012	11	164	84.95%
	MaxViT-L [31]	224	212M	43.9G	34	544	759	10	123	85.17%
	FasterViT-1 [32]	224	53M	5.3G	67	1123	4106	23	363	83.2%
	FasterViT-2 [32]	224	76M	8.7G	64	1112	4376	24	321	84.2%
	FasterViT-3 [32]	224	160M	18.2G	46	831	3131	17	257	84.9%
	FasterViT-4 [32]	224	425M	36.6G	50	800	1392	18	234	85.4%
Ours	AsCAN-T	224	55M	7.7G	199	3224	4295	67	1148	83.44%
	AsCAN-B	224	98M	16.7G	113	1878	2393	38	590	84.73%
	AsCAN-L	224	173M	30.7G	120	1381	1617	40	440	85.24%

Table 8: **Results on ImageNet-1K for Classification Task (memory consumption).** Following Tab. 7, for recent related networks, we include memory consumed during inference with 64 batch size.

	Architecture	Resolution	Params	MACs	Throughput (images/s) Batch (B)					Top-1 Accuracy	Memory (GB)
					A100			V100			
					B=1	B=16	B=64	B=1	B=16		B=64
ConvNet	RDNet-S [102]	224	50M	8.7G	102	1782	2761	53	780	83.7%	12.6
	RDNet-B [102]	224	87M	15.4G	80	1578	1891	48	589	84.4%	17.5
	RDNet-L [102]	224	186M	34.7G	78	640	990	32	290	84.8%	26.2
Hybrid	MOAT-2 [92]	224	73M	17.2G	132	1367	2087	38	424	84.7%	31.8
	MOAT-3 [92]	224	190M	44.9G	70	805	962	21	246	85.3%	65.2
	SMT-S [79]	224	21M	4.7G	38	566	2211	43	348	83.7%	13.5
	SMT-B [79]	224	32M	7.7G	27	388	1412	14	243	84.3%	22.6
	MogaNet-S [82]	224	25M	5.0G	93	1593	2455	47	740	83.4%	17.1
	MogaNet-L [82]	224	83M	15.9G	34	523	882	24	290	84.7%	46.6
	MogaNet-XL [82]	224	181M	34.5G	32	471	576	19	210	85.1%	74.9
	BiFormer-S [80]	224	26M	4.5G	45	937	2139	36	595	83.8%	18.6
	BiFormer-B [80]	224	57M	9.8G	50	840	1439	28	440	84.3%	27.9
	RMT-S [81]	224	27M	4.5G	46	790	2439	38	480	84.1%	13.7
Ours	AsCAN-T	224	55M	7.7G	199	3224	4295	67	1148	83.44%	9.6
	AsCAN-B	224	98M	16.7G	113	1878	2393	38	590	84.73%	15.2
	AsCAN-L	224	173M	30.7G	120	1381	1617	40	440	85.24%	21.2

Table 9: **Analysis of Architecture Configuration (with `T` before `C`).** We extend Tab. 2 by ablating over the preference of `C` and `T` blocks in a stage. Using **T** block in stem / early layers result in lower throughput. Further, the performance of configurations with **T** before **C** yields lower accuracy vs throughput trade-off.

Block Configuration	Params	Inference(images/s)			Top-1 Acc.
		A100		V100	
		B=16	B=64	B=16	
`CC-CCCT-CCTT-CTTT` (C1)	55M	3224	4295	1148	83.4%
`CC-CCCT-CCTT-CCTT` (C2)	73M	3217	4179	1036	83.2%
`CC-CCCT-CCTT-TTTT` (C3)	41M	3384	4472	1224	82.9%
`CC-CCCT-CCCC-TTTT` (C4)	50M	3434	4411	1182	83.1%
`CC-CCCT-CCCT-CCCT` (C5)	95M	3135	4066	991	82.7%
`CC-TCCC-CCTT-CTTT` (T1)	56M	3029	4021	945	82.8%
`CC-CCCT-TTCC-CTTT` (T2)	57M	3100	4092	1021	82.9%
`CC-CCCT-CCTT-TTTC` (T3)	64M	3190	4193	1045	83.1%
`TT-CCCT-CCTT-CTTT` (T4)	55M	1428	1584	487	83.1%
`TT-TTTC-TTCC-TTTC` (T5)	100M	1280	1440	390	83.5%

Table 10: **ImageNet-21K [72] Pre-training.** We report the performance of models pre-trained on ImageNet-21K with 224 resolution and fine-tuned on ImageNet-1K dataset. We report the inference latency as the throughput (images per second) that is measured by inferring images with batch size as B in half-precision, *i.e.*, fp16, on an A100 GPU using torch-compile and benchmark utility from timm library [100].

	Architecture	Resolution	Params	MACs	Batch (B=16) Throughput (images/s)	Batch (B=64) Throughput (images/s)	Top-1 Accuracy
	ConvNeXt-L [74]	224	198M	34.4G	1045	1127	86.6%
	MaxViT-L [31]	224	212M	43.9G	544	759	86.7%
	FasterViT-4 [32]	224	425M	36.6G	800	1392	86.6%
Ours	AsCAN-L	224	173M	30.7G	1381	1617	86.7%

Table 11: **Semantic Segmentation Results on ADE20K [104].** We compare different backbones on the ADE20K [104] semantic segmentation benchmark with UPerNet [106] as the detection architecture. Computational and storage statistics are computed using the input resolution of 512×512.

Backbone	**Latency (frames/s) A100**	**Latency (frames/s) V100**	**Params**	**MACs (G)**	**mIoU**
Swin-T [46]	44	23	60M	237	44.5
FasterViT-2 [32]	47	25	-	-	47.2
AsCAN-T (Ours)	64	30	86M	264	47.3
Swin-S [46]	27	16	81M	261	47.7
FasterViT-3 [32]	34	19	-	-	48.7
AsCAN-B (Ours)	44	24	128M	311	48.9
Swin-B [46]	23	13	121M	301	48.1
FasterViT-4 [32]	28	15	-	-	49.1
AsCAN-L (Ours)	36	19	204M	397	50.3

Table 12: **Resource Usage Comparison.** We compare the training time required to learn various diffusion models in the literature to our proposal. We also include parameter count and inference latency of these models.

Model	**Params**	**Train GPU A100 days**	**Inference per image** (512×512)	**Inference per image** (1024×1024)
RAPHAEL	3.0B	60,000	-	-
DALL.E 2	6.5B	41,667	-	-
Imagen	3.0B	7,132	-	13.3s
SDv1.5	0.9B	6,250	1.9s	-
SDXL+Refiner	2.6B	-	7.9s	12.2s
Wurstchen	1.0B	810	2.5s	-
GigaGAN	0.9B	4,783	-	
PixArt-α	0.6B	753	2.1s	7.2s
Ours	2.4B	2,688	2.2s	5.5s

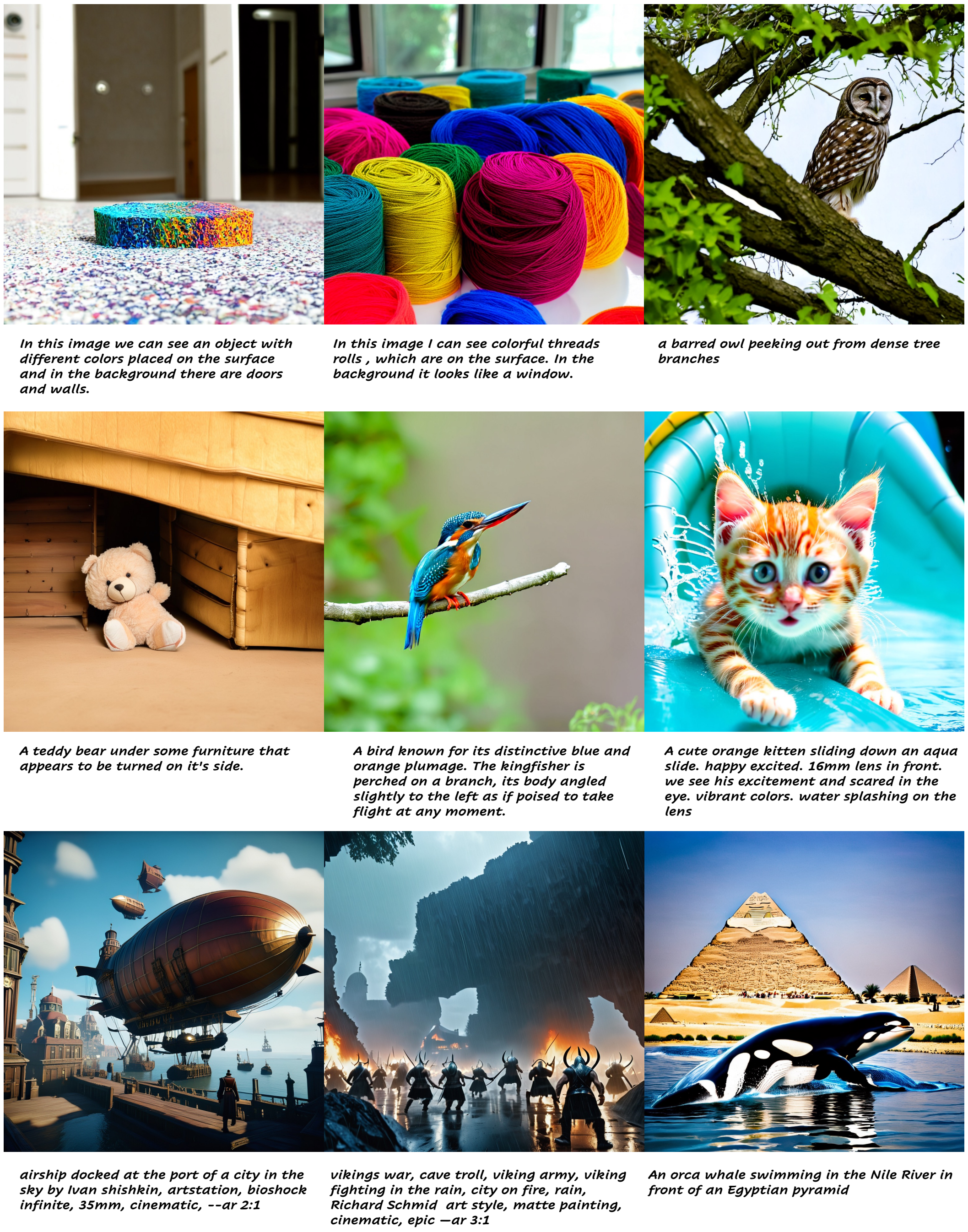

In this image we can see an object with different colors placed on the surface and in the background there are doors and walls.

In this image I can see colorful threads rolls , which are on the surface. In the background it looks like a window.

a barred owl peeking out from dense tree branches

A teddy bear under some furniture that appears to be turned on it's side.

A bird known for its distinctive blue and orange plumage. The kingfisher is perched on a branch, its body angled slightly to the left as if poised to take flight at any moment.

A cute orange kitten sliding down an aqua slide. happy excited. 16mm lens in front. we see his excitement and scared in the eye. vibrant colors. water splashing on the lens

airship docked at the port of a city in the sky by Ivan shishkin, artstation, bioshock infinite, 35mm, cinematic, --ar 2:1

vikings war, cave troll, viking army, viking fighting in the rain, city on fire, rain, Richard Schmid art style, matte painting, cinematic, epic —ar 3:1

An orca whale swimming in the Nile River in front of an Egyptian pyramid

Figure 10: Example text-to-image generation results.

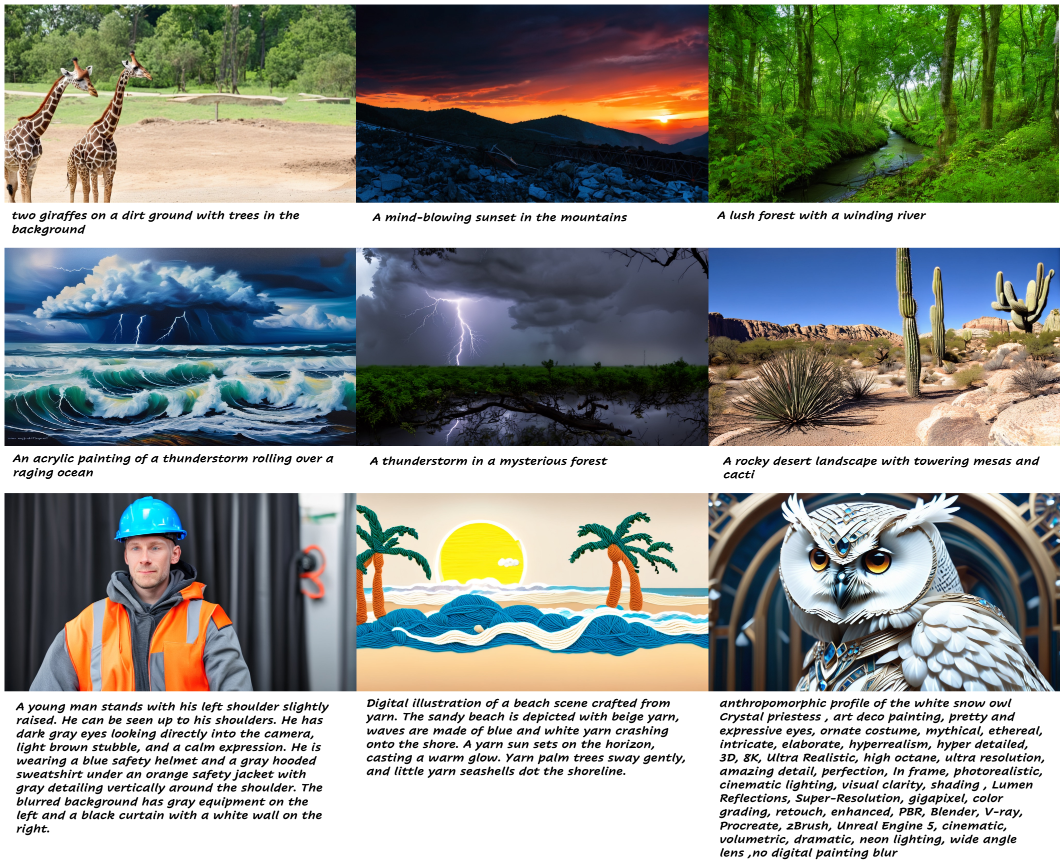

two giraffes on a dirt ground with trees in the background

A mind-blowing sunset in the mountains

A lush forest with a winding river

An acrylic painting of a thunderstorm rolling over a raging ocean

A thunderstorm in a mysterious forest

A rocky desert landscape with towering mesas and cacti

A young man stands with his left shoulder slightly raised. He can be seen up to his shoulders. He has dark gray eyes looking directly into the camera, light brown stubble, and a calm expression. He is wearing a blue safety helmet and a gray hooded sweatshirt under an orange safety jacket with gray detailing vertically around the shoulder. The blurred background has gray equipment on the left and a black curtain with a white wall on the right.

Digital illustration of a beach scene crafted from yarn. The sandy beach is depicted with beige yarn, waves are made of blue and white yarn crashing onto the shore. A yarn sun sets on the horizon, casting a warm glow. Yarn palm trees sway gently, and little yarn seashells dot the shoreline.

anthropomorphic profile of the white snow owl Crystal priestess , art deco painting, pretty and expressive eyes, ornate costume, mythical, ethereal, intricate, elaborate, hyperrealism, hyper detailed, 3D, 8K, Ultra Realistic, high octane, ultra resolution, amazing detail, perfection, In frame, photorealistic, cinematic lighting, visual clarity, shading , Lumen Reflections, Super-Resolution, gigapixel, color grading, retouch, enhanced, PBR, Blender, V-ray, Procreate, zBrush, Unreal Engine 5, cinematic, volumetric, dramatic, neon lighting, wide angle lens ,no digital painting blur

Figure 11: Example text-to-image generation results.

NeurIPS Paper Checklist

1. **Claims**

   Question: Do the main claims made in the abstract and introduction accurately reflect the paper's contributions and scope?

   Answer: [Yes]

   Justification: Our claims in the abstract and introduction regarding the efficiency and performance trade-offs of the asymmetrically distributed convolution-attention networks, reflect the paper's contributions. We design these new architectures for image recognition, semantic segmentation, and text-to-image applications. We show these applications and architecture modifications and advantages in our empirical evaluations.

   Guidelines:

   - The answer NA means that the abstract and introduction do not include the claims made in the paper.
   - The abstract and/or introduction should clearly state the claims made, including the contributions made in the paper and important assumptions and limitations. A No or NA answer to this question will not be perceived well by the reviewers.
   - The claims made should match theoretical and experimental results, and reflect how much the results can be expected to generalize to other settings.
   - It is fine to include aspirational goals as motivation as long as it is clear that these goals are not attained by the paper.

2. **Limitations**

   Question: Does the paper discuss the limitations of the work performed by the authors?

   Answer: [Yes]

   Justification: Yes. We describe the limitations in Appendix Sec. A.8.

   Guidelines:

   - The answer NA means that the paper has no limitation while the answer No means that the paper has limitations, but those are not discussed in the paper.
   - The authors are encouraged to create a separate "Limitations" section in their paper.
   - The paper should point out any strong assumptions and how robust the results are to violations of these assumptions (e.g., independence assumptions, noiseless settings, model well-specification, asymptotic approximations only holding locally). The authors should reflect on how these assumptions might be violated in practice and what the implications would be.
   - The authors should reflect on the scope of the claims made, e.g., if the approach was only tested on a few datasets or with a few runs. In general, empirical results often depend on implicit assumptions, which should be articulated.
   - The authors should reflect on the factors that influence the performance of the approach. For example, a facial recognition algorithm may perform poorly when image resolution is low or images are taken in low lighting. Or a speech-to-text system might not be used reliably to provide closed captions for online lectures because it fails to handle technical jargon.
   - The authors should discuss the computational efficiency of the proposed algorithms and how they scale with dataset size.
   - If applicable, the authors should discuss possible limitations of their approach to address problems of privacy and fairness.
   - While the authors might fear that complete honesty about limitations might be used by reviewers as grounds for rejection, a worse outcome might be that reviewers discover limitations that aren't acknowledged in the paper. The authors should use their best judgment and recognize that individual actions in favor of transparency play an important role in developing norms that preserve the integrity of the community. Reviewers will be specifically instructed to not penalize honesty concerning limitations.

3. **Theory Assumptions and Proofs**

Question: For each theoretical result, does the paper provide the full set of assumptions and a complete (and correct) proof?

Answer: [NA]

Justification: No theoretical results included in this work.

Guidelines:

- The answer NA means that the paper does not include theoretical results.
- All the theorems, formulas, and proofs in the paper should be numbered and cross-referenced.
- All assumptions should be clearly stated or referenced in the statement of any theorems.
- The proofs can either appear in the main paper or the supplemental material, but if they appear in the supplemental material, the authors are encouraged to provide a short proof sketch to provide intuition.
- Inversely, any informal proof provided in the core of the paper should be complemented by formal proofs provided in appendix or supplemental material.
- Theorems and Lemmas that the proof relies upon should be properly referenced.

4. **Experimental Result Reproducibility**

Question: Does the paper fully disclose all the information needed to reproduce the main experimental results of the paper to the extent that it affects the main claims and/or conclusions of the paper (regardless of whether the code and data are provided or not)?

Answer: [Yes]

Justification: We describe the architecture configurations used in this work in detail in the main and appendix sections. We also describe the hyper-parameter configurations used to train this model (training iterations, optimizer, learning rate, weight decay, data augmentation, etc.)

Guidelines:

- The answer NA means that the paper does not include experiments.
- If the paper includes experiments, a No answer to this question will not be perceived well by the reviewers: Making the paper reproducible is important, regardless of whether the code and data are provided or not.
- If the contribution is a dataset and/or model, the authors should describe the steps taken to make their results reproducible or verifiable.
- Depending on the contribution, reproducibility can be accomplished in various ways. For example, if the contribution is a novel architecture, describing the architecture fully might suffice, or if the contribution is a specific model and empirical evaluation, it may be necessary to either make it possible for others to replicate the model with the same dataset, or provide access to the model. In general. releasing code and data is often one good way to accomplish this, but reproducibility can also be provided via detailed instructions for how to replicate the results, access to a hosted model (e.g., in the case of a large language model), releasing of a model checkpoint, or other means that are appropriate to the research performed.
- While NeurIPS does not require releasing code, the conference does require all submissions to provide some reasonable avenue for reproducibility, which may depend on the nature of the contribution. For example
  (a) If the contribution is primarily a new algorithm, the paper should make it clear how to reproduce that algorithm.
  (b) If the contribution is primarily a new model architecture, the paper should describe the architecture clearly and fully.
  (c) If the contribution is a new model (e.g., a large language model), then there should either be a way to access this model for reproducing the results or a way to reproduce the model (e.g., with an open-source dataset or instructions for how to construct the dataset).
  (d) We recognize that reproducibility may be tricky in some cases, in which case authors are welcome to describe the particular way they provide for reproducibility. In the case of closed-source models, it may be that access to the model is limited in

some way (e.g., to registered users), but it should be possible for other researchers to have some path to reproducing or verifying the results.

5. **Open access to data and code**

   Question: Does the paper provide open access to the data and code, with sufficient instructions to faithfully reproduce the main experimental results, as described in supplemental material?

   Answer: [No]

   Justification: We plan to release our asymmetric architecture implementation for facilitating future research in this direction.

   Guidelines:

   - The answer NA means that paper does not include experiments requiring code.
   - Please see the NeurIPS code and data submission guidelines (`https://nips.cc/public/guides/CodeSubmissionPolicy`) for more details.
   - While we encourage the release of code and data, we understand that this might not be possible, so "No" is an acceptable answer. Papers cannot be rejected simply for not including code, unless this is central to the contribution (e.g., for a new open-source benchmark).
   - The instructions should contain the exact command and environment needed to run to reproduce the results. See the NeurIPS code and data submission guidelines (`https://nips.cc/public/guides/CodeSubmissionPolicy`) for more details.
   - The authors should provide instructions on data access and preparation, including how to access the raw data, preprocessed data, intermediate data, and generated data, etc.
   - The authors should provide scripts to reproduce all experimental results for the new proposed method and baselines. If only a subset of experiments are reproducible, they should state which ones are omitted from the script and why.
   - At submission time, to preserve anonymity, the authors should release anonymized versions (if applicable).
   - Providing as much information as possible in supplemental material (appended to the paper) is recommended, but including URLs to data and code is permitted.

6. **Experimental Setting/Details**

   Question: Does the paper specify all the training and test details (e.g., data splits, hyperparameters, how they were chosen, type of optimizer, etc.) necessary to understand the results?

   Answer: [Yes]

   Justification: We provide the experimental settings and details for experiments conducted in this work (see Sec. A.2, Sec. A.3, Sec. 3.3.2).

   Guidelines:

   - The answer NA means that the paper does not include experiments.
   - The experimental setting should be presented in the core of the paper to a level of detail that is necessary to appreciate the results and make sense of them.
   - The full details can be provided either with the code, in appendix, or as supplemental material.

7. **Experiment Statistical Significance**

   Question: Does the paper report error bars suitably and correctly defined or other appropriate information about the statistical significance of the experiments?

   Answer: [No]

   Justification: Similar to earlier works on ImageNet-1K and Text-to-Image generations, we do not report any error bars due to high computational resources involved in training one run.

   Guidelines:

   - The answer NA means that the paper does not include experiments.

- The authors should answer "Yes" if the results are accompanied by error bars, confidence intervals, or statistical significance tests, at least for the experiments that support the main claims of the paper.
- The factors of variability that the error bars are capturing should be clearly stated (for example, train/test split, initialization, random drawing of some parameter, or overall run with given experimental conditions).
- The method for calculating the error bars should be explained (closed form formula, call to a library function, bootstrap, etc.)
- The assumptions made should be given (e.g., Normally distributed errors).
- It should be clear whether the error bar is the standard deviation or the standard error of the mean.
- It is OK to report 1-sigma error bars, but one should state it. The authors should preferably report a 2-sigma error bar than state that they have a 96% CI, if the hypothesis of Normality of errors is not verified.
- For asymmetric distributions, the authors should be careful not to show in tables or figures symmetric error bars that would yield results that are out of range (e.g. negative error rates).
- If error bars are reported in tables or plots, The authors should explain in the text how they were calculated and reference the corresponding figures or tables in the text.

8. **Experiments Compute Resources**

   Question: For each experiment, does the paper provide sufficient information on the computer resources (type of compute workers, memory, time of execution) needed to reproduce the experiments?

   Answer: [Yes]

   Justification: Yes, we describe the amount of resources required to train our models, including the hardware type. We also provide the total number of iterations/epochs required to reproduce the reported results.

   Guidelines:

   - The answer NA means that the paper does not include experiments.
   - The paper should indicate the type of compute workers CPU or GPU, internal cluster, or cloud provider, including relevant memory and storage.
   - The paper should provide the amount of compute required for each of the individual experimental runs as well as estimate the total compute.
   - The paper should disclose whether the full research project required more compute than the experiments reported in the paper (e.g., preliminary or failed experiments that didn't make it into the paper).

9. **Code Of Ethics**

   Question: Does the research conducted in the paper conform, in every respect, with the NeurIPS Code of Ethics `https://neurips.cc/public/EthicsGuidelines`?

   Answer: [Yes]

   Justification: We have reviewed the code of ethics and our research work conforms to this code.

   Guidelines:

   - The answer NA means that the authors have not reviewed the NeurIPS Code of Ethics.
   - If the authors answer No, they should explain the special circumstances that require a deviation from the Code of Ethics.
   - The authors should make sure to preserve anonymity (e.g., if there is a special consideration due to laws or regulations in their jurisdiction).

10. **Broader Impacts**

    Question: Does the paper discuss both potential positive societal impacts and negative societal impacts of the work performed?

    Answer: [Yes]

Justification: We discuss the societal impacts of this work in the appendix Sec. A.9.

Guidelines:

- The answer NA means that there is no societal impact of the work performed.
- If the authors answer NA or No, they should explain why their work has no societal impact or why the paper does not address societal impact.
- Examples of negative societal impacts include potential malicious or unintended uses (e.g., disinformation, generating fake profiles, surveillance), fairness considerations (e.g., deployment of technologies that could make decisions that unfairly impact specific groups), privacy considerations, and security considerations.
- The conference expects that many papers will be foundational research and not tied to particular applications, let alone deployments. However, if there is a direct path to any negative applications, the authors should point it out. For example, it is legitimate to point out that an improvement in the quality of generative models could be used to generate deepfakes for disinformation. On the other hand, it is not needed to point out that a generic algorithm for optimizing neural networks could enable people to train models that generate Deepfakes faster.
- The authors should consider possible harms that could arise when the technology is being used as intended and functioning correctly, harms that could arise when the technology is being used as intended but gives incorrect results, and harms following from (intentional or unintentional) misuse of the technology.
- If there are negative societal impacts, the authors could also discuss possible mitigation strategies (e.g., gated release of models, providing defenses in addition to attacks, mechanisms for monitoring misuse, mechanisms to monitor how a system learns from feedback over time, improving the efficiency and accessibility of ML).

11. **Safeguards**

    Question: Does the paper describe safeguards that have been put in place for responsible release of data or models that have a high risk for misuse (e.g., pretrained language models, image generators, or scraped datasets)?

    Answer: [Yes]

    Justification: Yes, we discuss various safeguards both for preparing training data as well as serving the generated images for our text-to-image generation model.

    Guidelines:

    - The answer NA means that the paper poses no such risks.
    - Released models that have a high risk for misuse or dual-use should be released with necessary safeguards to allow for controlled use of the model, for example by requiring that users adhere to usage guidelines or restrictions to access the model or implementing safety filters.
    - Datasets that have been scraped from the Internet could pose safety risks. The authors should describe how they avoided releasing unsafe images.
    - We recognize that providing effective safeguards is challenging, and many papers do not require this, but we encourage authors to take this into account and make a best faith effort.

12. **Licenses for existing assets**

    Question: Are the creators or original owners of assets (e.g., code, data, models), used in the paper, properly credited and are the license and terms of use explicitly mentioned and properly respected?

    Answer: [Yes]

    Justification: For our image recognition and semantic segmentation experiments, we use the widely available ImageNet-1K and ADE20K datasets. We cite these resources in the work. For the T2I experiments, we use first party and licensed datasets. We depict this entire process in Fig. 6. We start by collating all these data sources to create a stream of images and if available, relevant text captions. Next stage, we add a series of filters to improve the quality of the selected images (resolution, de-duplication, aesthetic score, nsfw filtering, etc.). Since this data most contains very short description or almost non-existent description of the image, we unify the captioning process using an image captioning model. We collect a subset of 200K data for human annotations, where we ask the annotators to add details such as the <angle shot of the image>, <image background information>, <human attributes>, etc. We use this labelled data to fine-tune a BLIP2 model which is used to generate long captions similar to this format.

Guidelines:

- The answer NA means that the paper does not use existing assets.
- The authors should cite the original paper that produced the code package or dataset.
- The authors should state which version of the asset is used and, if possible, include a URL.
- The name of the license (e.g., CC-BY 4.0) should be included for each asset.
- For scraped data from a particular source (e.g., website), the copyright and terms of service of that source should be provided.
- If assets are released, the license, copyright information, and terms of use in the package should be provided. For popular datasets, `paperswithcode.com/datasets` has curated licenses for some datasets. Their licensing guide can help determine the license of a dataset.
- For existing datasets that are re-packaged, both the original license and the license of the derived asset (if it has changed) should be provided.
- If this information is not available online, the authors are encouraged to reach out to the asset's creators.

13. **New Assets**

    Question: Are new assets introduced in the paper well documented and is the documentation provided alongside the assets?

    Answer: [NA]

    Justification: No new assets introduced in this work.

    Guidelines:

    - The answer NA means that the paper does not release new assets.
    - Researchers should communicate the details of the dataset/code/model as part of their submissions via structured templates. This includes details about training, license, limitations, etc.
    - The paper should discuss whether and how consent was obtained from people whose asset is used.
    - At submission time, remember to anonymize your assets (if applicable). You can either create an anonymized URL or include an anonymized zip file.

14. **Crowdsourcing and Research with Human Subjects**

    Question: For crowdsourcing experiments and research with human subjects, does the paper include the full text of instructions given to participants and screenshots, if applicable, as well as details about compensation (if any)?

    Answer: [NA]

    Justification: Our research does not involve research with human subjects.

    Guidelines:

    - The answer NA means that the paper does not involve crowdsourcing nor research with human subjects.
    - Including this information in the supplemental material is fine, but if the main contribution of the paper involves human subjects, then as much detail as possible should be included in the main paper.
    - According to the NeurIPS Code of Ethics, workers involved in data collection, curation, or other labor should be paid at least the minimum wage in the country of the data collector.

15. **Institutional Review Board (IRB) Approvals or Equivalent for Research with Human Subjects**

Question: Does the paper describe potential risks incurred by study participants, whether such risks were disclosed to the subjects, and whether Institutional Review Board (IRB) approvals (or an equivalent approval/review based on the requirements of your country or institution) were obtained?

Answer: [NA]

Justification: Our research does not involve research with human subjects.

Guidelines:

- The answer NA means that the paper does not involve crowdsourcing nor research with human subjects.
- Depending on the country in which research is conducted, IRB approval (or equivalent) may be required for any human subjects research. If you obtained IRB approval, you should clearly state this in the paper.
- We recognize that the procedures for this may vary significantly between institutions and locations, and we expect authors to adhere to the NeurIPS Code of Ethics and the guidelines for their institution.
- For initial submissions, do not include any information that would break anonymity (if applicable), such as the institution conducting the review.